Combined silicon carbide and zirconia open cell foams for the process intensification of catalytic methane combustion in lean conditions: impact on heat and mass transfer

Combined silicon carbide and zirconia open cell foams for the process intensification of catalytic methane combustion in lean conditions: impact on heat and mass transfer

Carmen W. Moncada Quintero, Giuliana Ercolino, Stefania Specchia**

Politecnico di Torino, Department of Applied Science and Technology, Corso Duca degli Abruzzi 24, 10129 Torino, Italy

* Corresponding authors: carmen.moncada@polito.it, stefania.specchia@polito.it

Graphical Abstract

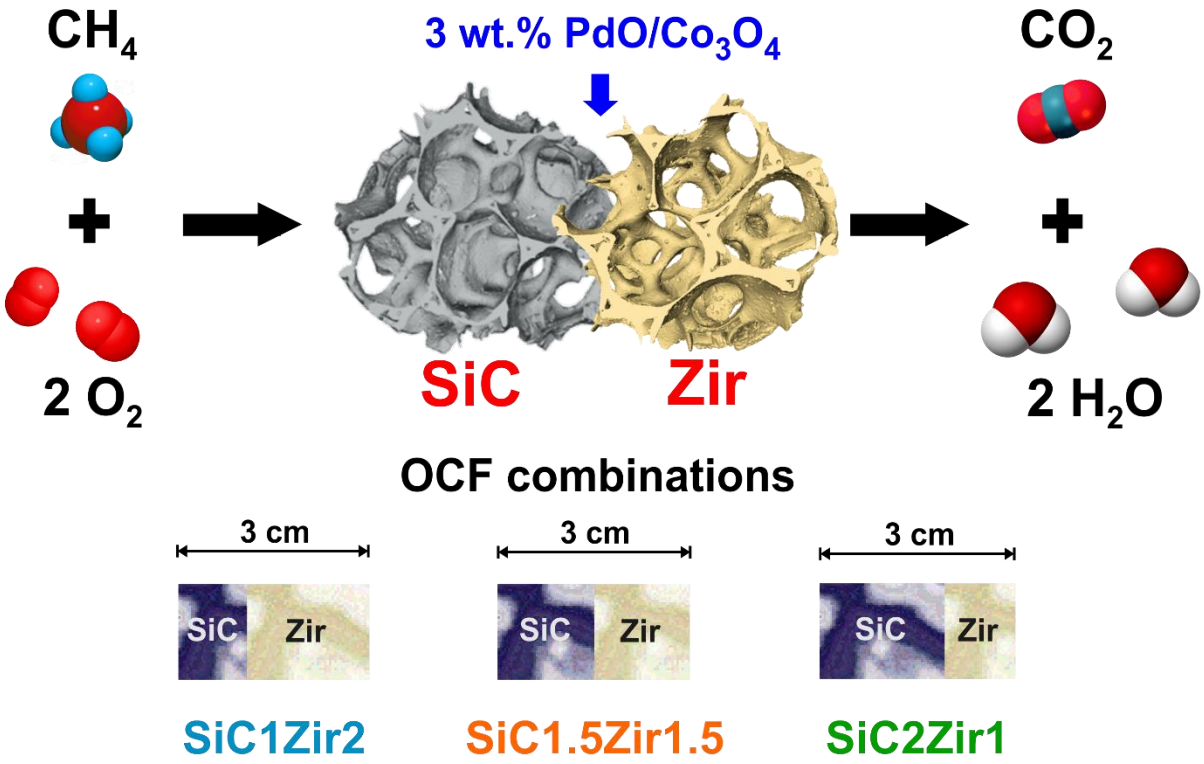

Keywords

Open cell foams; palladium; cobalt spinel; kinetic and mass transfer regimes; heat transfer effects.

Highlights

- Catalytic performance of 3% PdO/Co_3O_4 lined on various combinations of ceramic OCF
- Evaluation of apparent kinetic parameters for each foam combination.
- Kinetic, external and internal mass transfer resistances: Operating regimes.
- Effects of the external and internal heat transfer on combined OCF configurations
- Synergetic effect on catalytic activity with same length OCFs in the order SiC+Zir

Abstract

For catalytic process intensification, a series of open cell foams (OCFs) made of silicon carbide (SiC) and zirconia (Zir) with pore density of 30 ppi coated with 3 wt.% PdO/Co_3O_4 as catalyst were combined together and tested toward methane oxidation in lean conditions. In each combination, the SiC OCF was positioned in the reactor on the inlet side of the reactant gases followed by the Zir OCF. The reactor was fed at different weight hourly space velocities (WHSV, 30 and 90 NL h^{-1} g_{cat}^{-1}) and inlet methane concentrations (0.5 and 1 vol.%). The best results are obtained with the combination where two supports of same length but with different thermal conductivity (higher at the inlet of the reactor, SiC, and lower at the outlet, Zir) are used in series. For all OCF combinations, mass transfer effects were evaluated using the characteristic resistances (kinetic, internal and external mass transfer). The external and internal heat transfer effects were analyzed using the Mears and Anderson criteria. Furthermore, a comparison in terms of volumetric heat transfer coefficient and heats of removal/reaction was performed.

1. Introduction

Methane (CH_4), the main component of natural gas, is one of the most important gases that contributes to the greenhouse effect. Although CH_4 is about 200 times less abundant in the atmosphere than carbon dioxide (CO_2), its ability to absorb thermal infrared radiation is much

more effective and, as a consequence, its impact on the greenhouse effect is much stronger compared to that of CO_2 [1,2]. In fact, the global warming potential (GWP) of CH_4 is 86 over a 20-year period, and 28 over a 100-year period (by definition, the GWP CO_2 is 1) [3]. Indeed, CH_4 emissions recorded an increase of more than 150% since 1750 as a result of human activities [4]. By the end of 2019, the global average concentration of CH_4 in the atmosphere reached about 1875 parts per billion (ppb), more than two and a half times pre-industrial levels [5]. Methane emissions come mainly from anthropogenic sources such as agriculture, energy, industry and waste management processes [6,7]. Most of the human-induced emissions have low CH_4 concentrations, generally between 0.1-1 vol.% [8–10]. Reducing CH_4 emissions could offer a great opportunity to mitigate global climate change leading to significant environmental and economic benefits.

Despite the high stability of the CH_4 molecule, the catalytic combustion is considered one of the most efficient and promising technologies to eliminate CH_4 emissions and maximize the use of rational and clean low-temperature energy. Therefore, the development of a catalyst with outstanding catalytic activity (the lowest possible shut-down temperature~~s~~) and high stability even at low temperature operations remains a challenge for chemical engineers. So far, Pd-based catalysts have been reported to be the most active catalytic systems for total oxidation of CH_4, due to their high activity at low temperature [11–15]. However, because of the relatively high cost associated with Pd, researchers have paid much attention to the study of alternative catalytic systems with a reduced amount of Pd, such as oxides or mixed oxides [16–18] and perovskites [19–21], because of their much lower cost and relatively abundant availability. In all cases, the nature of the catalyst carrier as well as the active phase-support interactions play a crucial role in the catalytic properties of Pd-based catalysts Recently, spinel cobalt oxide (Co_3O_4) has proven to be one of the best multifunctional materials for a wide variety of technological applications thanks to its surface redox reactivity properties, strong oxygen

mobility and lower Co–O binding energy [24–27]. Specifically, when CH_4 is oxidized, Co_3O_4 favors the removal of hydroxyl species from the PdO surface [28]. In this way, the active sites are more prone to CH_4 activation [15]. Besides, Co_3O_4 provides lattice oxygen to the PdO phase, favoring again the recreation of active sites afterwards [29]. This makes Co_3O_4 an optimal catalytic support, especially for the complete CH_4 oxidation in lean conditions, in comparison with other carriers such as Al_2O_3 or perovskites [11,12,22].

Currently, the attention has been focused on structured reactors as a potential way to facilitate the intensification of the process, thanks to the possibility of enhancing transport phenomena (increased mass and heat transfer rates [30–39]), bringing to significant benefits in terms of process efficiency, improved safety, and lower capital costs [40,41]. Open cell foams (OCFs) have become promising candidates owing to their attractive characteristics such as large specific surface area, high porosity, great mechanical strength and light-weight, as well as reduced pressure drops when compared to classical fixed-bed reactors [42–51]. In addition, their particular structural geometry produces a tortuous flow path that allows improving the reactive mixing and thus the transport properties.

Recently, we investigated the catalytic oxidation of CH_4 under lean conditions of 3 wt.% PdO/Co_3O_4 catalyst supported on individual OCFs made of silicon carbide (SiC), alumina (Alu) and zirconia (Zir) [52–55] with different pore density. Furthermore, a mass and heat transfer analysis was performed for each catalytic support [52]. We found that the best catalytic performance towards complete CH_4 conversion was obtained with the Zir OCF system [54]. Nevertheless, the higher thermal conductivity of the SiC OCF led to higher volumetric heat exchange coefficients, which help to hold the reaction heat and, consequently, provide the necessary energy to maintain the reaction during the extinction by delaying the shut-down temperature of the reactor [54], thanks to the existence of multiple steady-states [56–59]. In fact, although the best catalytic performance was obtained with the Zir OCF, the reaction

kinetics was favored in the SiC OCF showing a lower temperature range under kinetic control [52]. In the present work, we exploited the results obtained in our previous research by evaluating the catalytic performance of 3 wt.% PdO/Co_3O_4 catalyst towards CH_4 oxidation in lean conditions using three different combinations of OCFs made of SiC and Zir. The total length of each foam combination was 3 cm (as in our previous works [52–55]), while the lengths of each single OCF (SiC and Zir) were varied from 1, 1.5, and 2 cm. Each combination was placed inside the reactor with the SiC OCF always at the inlet side of the reactant gases. Thus, we tried three different bed configurations: SiC1Zir2, SiC1.5Zir1.5, SiC2Zir1. The idea of using the SiC OCF in the front matured from our previous experience, comparing the performance of PdO/Co_3O_4 on single Zir or SiC. We noticed that the reactor configuration with the SiC was able to guarantee a very good performance at low temperature, that is at the extinction of the combustion reaction [54]. In fact, recently, the study of ignition and extinction pathways in non-isothermal reactors is gaining importance to reach a better reactor's thermal management [59,60]. In this work, the reactor was fed at different weight hourly space velocities (WHSV) and inlet CH_4 concentrations. Moreover, the overall catalytic process resistance was evaluated in terms of kinetic, external, and internal mass transfer resistance allowing the identification of the operating regime of each OCF combination. Finally, heat transfer effects both within the catalyst and associated to the gas phase were analyzed.

2. Materials and methods

2.1. Open cell foams and chemicals

Ceramic OCFs made of Zirconia (Vukopor® HT30, labelled Zir OCF) and silicon carbide (Vukupor® S30, labelled SiC OCF) with pore density of 30 ppi (pore per inch) were purchased from Lanik s.r.o (Czech Republic) in dimensions of 0.9 cm as in diameter and 3 cm as length. For experimental purposes, the length of the foams was carefully reduced to 1, 1.5, and 2 cm,

obtaining the following OCF pieces: SiC1, SiC1.5, SiC2, Zir1, Zir1.5, and Zir2 (where each value indicates the foam length in cm). **Table 1** lists the textural properties of single SiC and Zir OCF of 30 ppi measured in our previous work using the X-ray computed micro-tomography technique [61].

Table 1. Textural properties of individual SiC and Zir OCF with pore density of 30 ppi [61].

	SiC OCF	**Zir OCF**
Pore diameter, d_p (mm)	2.22	2.87
Strut diameter, d_s (mm)	0.35	0.51
Open porosity, ε_o (-)	0.79	0.84
Specific surface area, S_{ga} (mm^{-1})	0.90	1.09

All reagents were purchased from Sigma-Aldrich: Cobalt(II) nitrate hexahydrate $Co(NO_3)_2 \cdot 6H_2O$ (≥98% purity), palladium(II) nitrate hydrate $Pd(NO_3)_2 \cdot xH_2O$ (≥99% purity), glycine NH_2CH_2COOH (≥99% purity), ethanol CH_3CH_2OH (≥99.8% purity), and acetone CH_3COCH_3 (≥99.8% purity). Ultrapure water obtained from a Millipore Milli-Q system with resistivity of ~18 MΩ cm was used to prepare all aqueous solutions. Catalytic tests were carried out using pure methane, oxygen and nitrogen gases (99.999% purity) supplied in cylinders provided by SIAD S.p.A.

2.2. Preparation of the foam structured catalysts

Prior to use, all foam pieces were washed in a water/acetone solution (50:50, v/v) for 30 min using an ultrasonic bath at room temperature and dried at 140 °C for 60 min. The deposition of

PdO/Co_3O_4 catalyst on each foam piece was performed in two consecutive steps, described in detail in our previous works [52–55]: i) solution combustion synthesis (SCS) method to deposit the Co_3O_4 carrier and ii) wetness impregnation (WI) of the PdO active phase. Briefly, each OCF piece was immersed in a 3 M aqueous solution of cobalt nitrate and glycine (with a ratio of glycine to stoichiometric amount of 0.25) for 3 minutes. The excess solution was removed from the foams with a flow of compressed air. Then, the wet OCFs were introduced into a muffle furnace preheated to 250 °C for 20 minutes to allow ignition of the combustion reaction. The coating operation was repeated several times until the desired Co_3O_4 carrier amount was achieved on each OCF. Once the foams were coated, they were calcined at 600 °C for 4h in static air. Subsequently, 3 wt.% PdO was deposited on the Co_3O_4-coated OCF pieces by WI. Through WI, each OCF was dipped several times in an aqueous solution containing the targeted amount of PdO. For each dipping, the OCF was rotated with tweezers, to ensure homogeneous absorption, and dried in a muffle at 140 °C for 1 h to remove water. The dipping/drying steps were repeated till the becker containing the aqueous solution was fully empty. Finally, the PdO/Co_3O_4 OCFs were calcined at 600 °C for 4h in static air. Considering that the three SiCZir OCF combinations were different in the length of each single foam (SiC1Zir2, SiC1.5Zir1.5, SiC2Zir1), but equal in terms of overall length (3 cm), for sake of comparison we deposited on each entire system a targeted amount of Co_3O_4+PdO equal to approx. 250 mg (PdO: 3 wt.% of the Co_3O_4 amount [52–55]), proportionally shared on the two single SiC or Zir OCF depending on their respective lengths in the SiCZir configuration.

2.3. Catalytic tests toward CH_4 combustion

Figure 1 shows the test rig we used for testing the CH_4 catalytic activity. A fixed bed reactor consisting of a straight quartz tube (10 mm inner diameter) placed inside a PID-controlled electric furnace was used for this purpose. The total length of all foam configurations was 3 cm,

with the SiC OCF positioned always at the inlet of the reactive gases followed by the Zir one. Each foam configuration was wrapped all along the length in a thin vermiculite foil to avoid channeling and heat dispersion phenomena at the reactor's wall/OCF boundary, especially at the SiCZir junction.

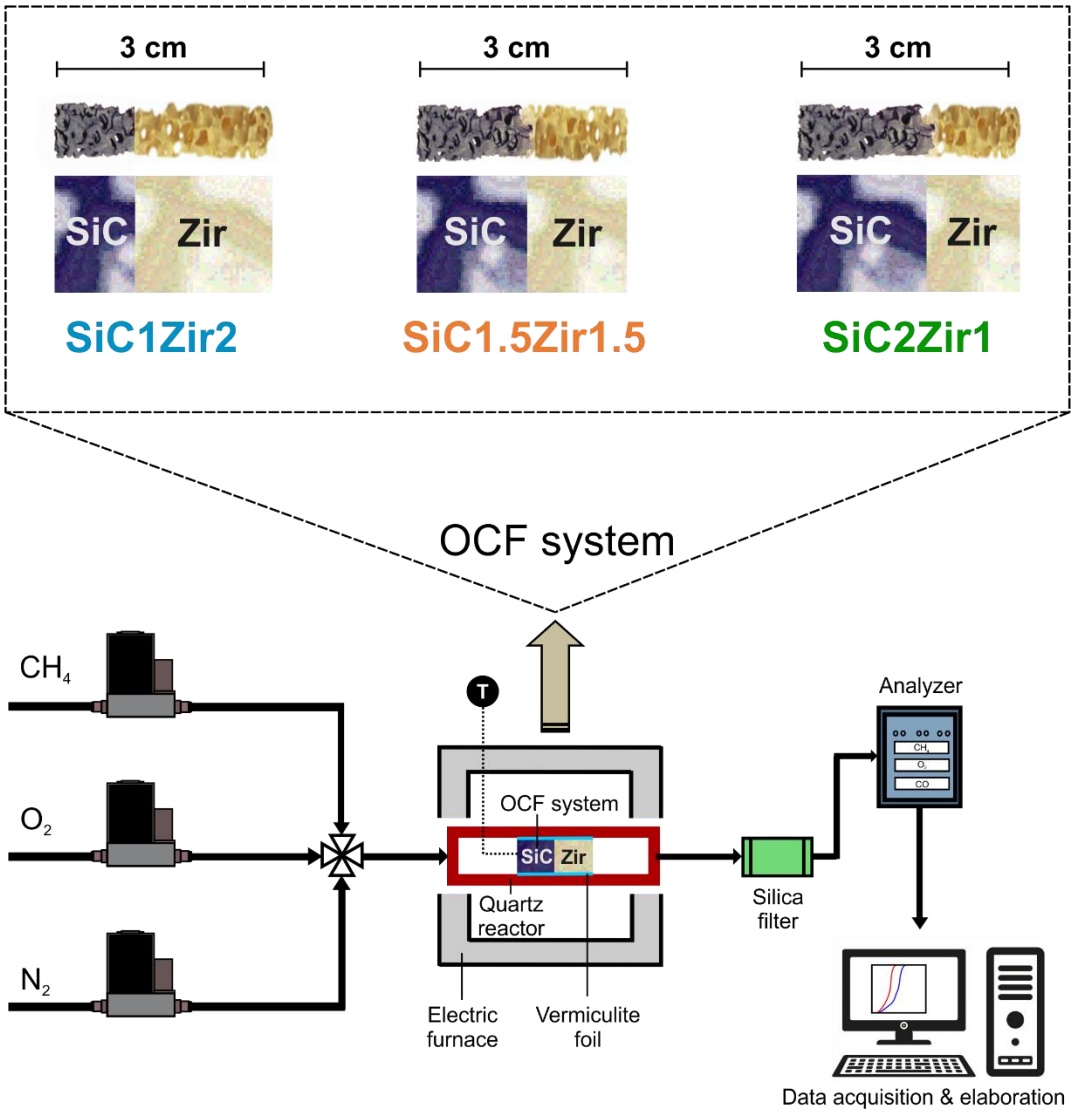

Figure 1. Schematic diagram of the lab-scale plant for CH_4 oxidation and the three combinations of ceramic OCFs made of SiC and Zir with pore density of 30 ppi used in this study.

The reactor was fed with a reactive $CH_4/O_2/N_2$ gas mixture, at methane concentrations of 0.5 or 1 vol.%, with a constant molar ratio of O_2/CH_4 equal to 8 to ensure lean conditions. First, the

reactor was heated to 700 °C (10 °C min^{-1}) while the reactant gas mixture was fed, to favor the ignition and the achievement of stationary conditions. Once the steady state conditions were reached (hold time at 700 °C for 1 h), the reactor was cooled to room temperature (5 °C min^{-1}), while the outlet dry gas concentration was monitored as a function of the temperature (measured by a K-type thermocouple located a few mm inside the inlet side of each foam configuration) using an ABB analyzer equipped with a Uras 14 NDIR module for $CO/CO_2/CH_4$ and a Magnos 106 paramagnetic module for O_2. Consequently, all the conversion versus temperature curves presented in this work are extinction curves, because of the more favorable CH_4 conversion profiles due to the presence of the ignition/extinction hysteresis (multiple steady states conditions [53,59]). The water vapor generated by the reaction was removed before entering the analyzer in a condenser set at 3 °C. The reagent flow rate was varied to allow the catalytic tests to be carried out at (WHSV) of 30 and 90 NL h^{-1} g_{cat}^{-1}. All catalytic runs were repeated at least three times to ensure reproducibility of the results.

2.3 Determination of the apparent kinetic parameters

The kinetics of CH_4 combustion can be approximated as a pseudo-first order reaction ($R^{obs} = k \cdot C_{CH_4}$) considering that all catalytic tests towards CH_4 oxidation performed on each PdO/Co_3O_4/SiCZir combination were conducted in a large excess of oxygen ($C_{O_2} \gg C_{CH_4}$). Thus, assuming a plug flow reactor model, the observed rate constant per unit of catalyst bulk density (k') for a first-order reaction was determined as:

$$k'(T) = \frac{1}{\tau} \cdot \ln\left(\frac{1}{1-X_{CH4}}\right) \quad (1)$$

$$\tau = \frac{W_{cat} \cdot C_{CH4}^{in}}{F_{CH4}^{in}} \quad (2)$$

where τ is the contact time (g_{cat} s m^{-3}), X_{CH4} is the CH_4 conversion, W_{cat} is the weight of PdO/Co_3O_4 catalyst (g_{cat}), and C_{CH4}^{in}, F_{CH4}^{in} are the inlet concentration (mol m^{-3}), and molar flow of methane (mol s^{-1}), respectively.

Then, the k' was plotted as a function of inverse temperature using the logarithmic form of the Arrhenius equation (**Equation 3**). The pre-exponential factor (A_o) and the apparent activation energy (E_{app}) were determined using the experimental data points with CH_4 conversion below 10%, that is, in kinetic regime.

$$k' = A_o \cdot e^{-\frac{E_{app}}{R_g \cdot T}} \;\; ; \;\; ln(k') = ln(A_o) - \frac{E_{app}}{R_g} \cdot \frac{1}{T} \tag{3}$$

2.4. External and internal mass transfer evaluation

The overall mass transfer process in a structured catalyst is usually bounded by two limits: external mass transfer from the bulk of the fluid phase to the external catalyst surface and internal mass transfer with chemical reaction into the catalytic thickness [30,31,33,40,49,62–68]. The external mass transfer is simplified using the classical concept of mass transfer coefficient, based on the assumption that all the resistance to mass transfer resides in a fictitious thin film in which the concentration gradients occur, while the diffusion and reaction processes are simplified using the concept of effectiveness factor [40,63]. Balakotaiah in 2008 [69], demonstrated that it was possible to use an internal mass transfer coefficient to simplify the diffusion and reaction process in a catalyst particle utilizing a hypothetical film model similar to that of external mass transfer. Later, Joshi et al. [70–73] extended this approach by developing a low dimensional model to describe convection processes with diffusion and reaction in washcoated monoliths of arbitrary shape. The main advantage of this model is that it allows the inclusion of intraparticle diffusional effects without explicitly solving the multicomponent diffusion-reaction problem within the catalyst layer.

Recently, we adapted the model developed by Joshi et al. [70–73] to evaluate the mass transfer effects that occur from the bulk of the gas phase to the outer catalyst surface and to the inside of the catalytic layer in single coated OCFs made of alumina, silicon carbide, and zirconia [52]. Briefly, the total mass transfer resistance (${R_m}^t$) can be described as the combined effect of two diffusive contributions using a series approach, as follows [52,53,71,72]:

$${R_m}^t = {R_m}^e + {R_m}^i \tag{4}$$

$${R_m}^t = \frac{1}{{k_m}^t}; \quad {R_m}^e = \frac{1}{{k_m}^e} = \frac{4 \cdot R_{\Omega e}}{Sh_{OCF} \cdot D_f} \quad ; \quad {R_m}^i = \frac{1}{{k_m}^i} = \frac{R_{\Omega,i}}{Sh_c \cdot D_e} \tag{5}$$

where ${R_m}^e$, ${R_m}^i$ are the gas phase film and intraparticle (within the PdO/Co_3O_4 catalyst layer) mass transfer resistances (s m^{-1}); ${k_m}^t$, ${k_m}^e$, ${k_m}^i$ are the total, external and internal mass transfer coefficients (m s^{-1}); $R_{\Omega e}$, $R_{\Omega,i}$ are the characteristic length scales for the transverse diffusion associated with the gas phase and the catalytic layer (m); D_f, D_e are the molecular and effective diffusivity of CH_4 in the fluid phase and within the catalyst layer (m^2 s^{-1}), and Sh_{OCF}, Sh_c are the external and internal Sherwood numbers.

The characteristic length scales are defined as the ratio of the flow or coated layer cross-sectional area to the gas-solid interfacial perimeter (wetted surface, assuming a continuous catalyst layer), which are expressed as:

$$R_{\Omega,e} = \frac{A_{\Omega,e}}{P_\Omega} = \frac{d_h}{4} \tag{6}$$

$$R_{\Omega,i} = \frac{A_{\Omega,i}}{P_\Omega} = \delta_c \tag{7}$$

where P_Ω is the wetted gas–coated layer interfacial perimeter (m); d_h is the hydraulic diameter of the foam (m); δ_c is the catalytic thickness (m); $A_{\Omega,e}$ and $A_{\Omega,i}$ are the cross sectional areas for the gas phase and coated catalyst layer (m^2); respectively.

To estimate the dimensionless external mass transfer coefficient (Sh_{OCF}), we use the correlation derived by Garrido et al. [74] for ceramic OCFs with circular strut shape valid for a voidage range of $0.75 \leq \varepsilon_{ocf} \leq 0.85$ and pore diameter of $0.87 \leq d_{p,c} \leq 3.13$ mm:

$$Sh_{OCF} = 1.0 \cdot Re^{0.47} \cdot Sc^{\frac{1}{3}} \cdot F_g \quad (8)$$

where Re is the Reynold number, Sc is the Smith number and F_g is the geometrical factor which depends on the pore diameter ($d_{p,c}$) and the OCF voidage (ε_{ocf}).

On the other hand, the dimensionless mass transfer coefficient within the catalyst layer (Sh_c) was estimated using the correlation derived by Joshi et al. [71] on washcoated monolith for first order reactions as:

$$Sh_c = Sh_{c,\infty} + \frac{\Lambda \cdot \phi^2}{1+\Lambda \cdot \phi} \quad (9)$$

where $Sh_{c,\infty}$is the asymptotic internal Sherwood number (where the pore diameter and coated layer shape was assumed to be circular, thus, $Sh_{c,\infty} = 3.013$) [75], Λ is a constant that depends on the coated layer geometry (for a circular coated layer shape with circular crown ratio of 1.1, $\Lambda = 0.38$) [71,72], and ϕ is the Thiele modulus for a first order reaction.

2.5. Overall catalytic performance: Kinetic and mass transfer regimes

To evaluate the operating regimes (kinetic, internal and external mass transfer) of the catalytic process, we used the low-dimensional model developed by Joshi et al. [70–72], considering the following assumptions: i) fully developed laminar flow; ii) very high axial Peclet number; iii) isothermal foam; and iv) first order reaction kinetics. In this way, the operating regime of each catalytic OCF combination was evaluated as the sum of the total mass transfer resistance and the reaction resistance as:

$$R^{ov} = {R_m}^t + R_r \quad (10)$$

Substituting the **Equation 4** in **10**, we obtain that:

$$R^{ov} = {R_m}^e + {R_m}^i + R_r \quad (11)$$

$$\frac{1}{k^{ov}} = \frac{1}{{k_m}^e} + \frac{1}{{k_m}^i} + \frac{1}{k \cdot R_{\Omega,i}} \quad (12)$$

where **Equations 11** and **12** describe the overall resistance of the catalytic process.

The Thiele modulus (ϕ) and the effectiveness factor (η) for a first order reactions were estimated as follows [71,72]:

$$\phi = \sqrt{\frac{k \cdot {R_{\Omega i}}^2}{D_e}} \tag{13}$$

$$\eta = \frac{1}{1+\frac{\phi^2}{Sh_c}} \tag{14}$$

2.6. External and internal heat transfer evaluation

In highly exothermic reactions, such as CH_4 combustion, additional to mass transfer limitations, temperature gradients can also originate both between the bulk fluid phase and the external catalyst surface (external heat transfer) and within the catalyst layer (internal heat transfer), causing catalyst deactivation due to thermal sintering [60]. Therefore, heat management becomes a key aspect for both reactor design and catalytic process control.

First of all, we estimated the volumetric heat transfer coefficients (h_e^v) of each OCF combination, which take into account the heat exchange between the fluid and outer catalyst surface. These are also influenced by the foam solid network that, as reported in our previous work [61], are composed of circular hollow struts, showing a macro/microporous skeleton with irregular and tortuous pathways. Thus, the h_e^v values were estimated using the correlation derived by Younis and Viskanta in 1993 [76] valid for ceramic OCFs with pore densities up to 70 ppi, as:

$$Nu = \frac{h_e^v \cdot d_{p,c}^2}{\lambda_f} = C \cdot Re^m \tag{15}$$

$$C = 0.819 \cdot \left[1 - 7.33 \cdot \left(\frac{d_{p,c}}{L}\right)\right] \tag{16}$$

$$m = 0.36 \cdot \left[1 + 15.5 \cdot \left(\frac{d_{p,c}}{L}\right)\right] \tag{17}$$

where Nu is the Nusselt number, λ_f is the gas phase thermal conductivity (W m^{-1} K^{-1}), C and m are geometrical parameters that depend on the OCFs, and L is the total length of each OCF combination (0.03 m)

To evaluate the effects of external heat transfer, we used the criterion proposed by Mears in 1971 [77], which assumes that the fluid phase heat transfer resistance is lumped at the surface, according to the following expression:

$$\chi = \left|\frac{(-\triangle H_r)\cdot R^{obs}\cdot R_{\Omega e}}{h_e\cdot T_b}\right| < \frac{0.15}{\gamma_b} \quad ; \quad \gamma_b = \frac{E_{app}}{R_g\cdot T_b} \tag{18}$$

where ΔH_r is the heat of CH_4 combustion reaction (J mol^{-1}), h_e is the heat transfer coefficient associated for the gas phase (W m^{-2} K^{-1}), T_b is the temperature in the bulk of the gas phase (K); γ_b is the Arrhenuis number evaluated at the bulk of the gas phase, R_g is the universal gas constant (J mol^{-1} K^{-1}), and χ is the Damköhler for interphase heat transport [63,77].

Thermal gradients within the catalyst layer were evaluated using the criterion proposed by Anderson in 1963 [78]:

$$\psi = \left|\frac{\left(-\triangle H_r\cdot R^{obs}\cdot R_{\Omega i}^2\right)}{\lambda_e\cdot T_s}\right| < \frac{0.75}{\gamma_s}; \quad \gamma_s = \frac{E_{app}}{R_g\cdot T_s} \tag{19}$$

where λ_e is the effective thermal conductivity (W m^{-1} K^{-1}), T_s is the temperature at the surface of the catalyst layer (K), γ_s is the Arrhenuis number evaluated at the surface of the gas phase, and ψ is the Damköhler for intraparticle heat transport [63].

Furthermore, the reaction and removal heats were evaluated at steady state conditions. Under these conditions, the heat released by the combustion reaction on any element on the outer surface of the PdO/Co_3O_4 catalyst layer must be transported from the catalyst surface to the bulk gas. Therefore, the heat analysis in steady state conditions, assuming a pseudo-first order reaction, is given as follows [40]:

$$Q_r = Q \tag{20}$$

$$Q_r = (R'_{CH4}) \cdot (-\Delta H_r) = A'_o \cdot e^{\left(-\frac{\gamma_b}{\theta+1}\right)} \cdot C_{CH4} \cdot (-\Delta H_r) \tag{21}$$

$$Q = h_e \cdot a_m \cdot (T_s - T_b) = h_e \cdot a_m \cdot T_b \cdot \theta \tag{22}$$

$$\theta = \frac{T_s - T_b}{T_b} \tag{23}$$

where Q_r is the heat generation rate per unit mass of catalyst (J Kg^{-1} s^{-1}), Q is the heat removal rate per unit mass of catalyst (J Kg^{-1} s^{-1}), R'_{CH4} is the reaction rate expressed with respect to CH_4 per unit mass of catalyst (mol Kg^{-1} s^{-1}), A'_o is the pre-exponential factor per unit of the catalyst bulk density (m^3 Kg^{-1} s^{-1}), a_m is the external surface area per unit mass of catalyst (m^2 Kg^{-1}), and θ is the dimensionless temperature.

Further, the relationship between the degree of external mass transfer control and the temperature difference between the bulk gas phase and the outer catalyst surface can be easily derived for steady-state conditions. Under such conditions, the CH_4 external mass transfer rate must be equal to the CH_4 conversion rate by surface reaction. Thus, assuming that the outer surface of the catalytic layer is uniformly accessible to the reactive gases, each section of the surface behaves kinetically the same:

$$k_m{}^e \cdot a_m \cdot (C_{CH_4,b} - C_{CH_4,s}) \cdot (-\Delta H_r) = h_e \cdot a_m \cdot (T_s - T_b) \tag{24}$$

Hence, solving for the temperature difference and considering the Chilton-Colburn analogies between heat and mass transfer by means of the j-factor correlations ($j_H \approx j_D$) leads to [79–81]:

$$(T_s - T_b) = \left(\frac{-\Delta H_r}{\rho_f \cdot c_{p,f}}\right) \cdot (C_{CH_4,b} - C_{CH_4,s}) \tag{25}$$

$$(T_s - T_b) = \left(\frac{-\Delta H_r \cdot C_{CH_4,b}}{\rho_f \cdot c_{p,f}}\right) \cdot Ca \tag{26}$$

where ρ_f is the density of gas mixture (kg m^{-3}), $c_{p,f}$ is the heat capacity per unit mass of gas mixture (J Kg^{-1} K^{-1}), $C_{CH_4,b}$ and $C_{CH_4,s}$ are the bulk gas and surface concentration of CH_4 and Ca is the Carberry number [63].

Now, introducing the definition of adiabatic temperature, **Equation 26** can be written as:

$$(T_s - T_b) = \Delta T_{ad} \cdot Ca \tag{27}$$

$$\Delta T_{ad} = \frac{-\Delta H_r \cdot C_{CH_4,b}}{\rho_f \cdot c_{p,f}} \quad ; \quad Ca = \frac{C_{CH_4,b} - C_{CH_4,s}}{C_{CH_4,b}} \tag{28}$$

Note that $(T_s - T_b)$ is maximum for reactions limited by mass transfer $Ca \geq 1$.

3. Results and discussion

The physical-chemical characterization of the combined OCFs, as well as the adhesive properties of the coated 3 wt.% PdO/Co_3O_4 on both SiC and Zir supports have been fully performed and reported in our previous works [52–55,61]. In fact, a series of sonication tests (not reported here, but available on our above-mentioned works) demonstrated that the layer of PdO/Co_3O_4 remains well attached to the ceramic OCFs, with practically no loss of catalyst from the surface of the foams after 2 h of sonication at 40 kHz. Thus, here we can affirm that the SCS + WI impregnation method allowed us to line on the two OCFs the desired PdO/Co_3O_4 catalyst, realizing a structured catalyst.

3.1. Catalytic tests toward CH_4 combustion

Figure 2 shows the extinction curves of CH_4 combustion for all flow conditions and coated SiCZir combinations studied. An increase in WHSV reduces the contact time between the reactants and the catalyst, which leads to a worsening of the catalytic performance. Thus, the CH_4 conversion cannot be maintained at low temperature and the extinction temperature shifts to slightly higher values. For both inlet CH_4 concentrations, when the reactor was operated at WHSV of 30, all SiCZir OCF combinations achieved complete conversion. Particularly, the

SiC1.5Zir1.5 started the extinction of the reaction at 221 °C (0.5 vol.% inlet CH_4 concentration) or 266 °C (1 vol.% inlet CH_4 concentration), followed by the SiC1Zir2 at 259 or 328 °C, respectively, and the SiC2Zir1 at 496 or 484 °C, respectively. By increasing the WHSV to 90, only the combinations SiC1Zir2 and SiC1.5Zir1.5 were able to maintain full CH_4 conversion, while the SiC2Zir1 combination, did not reach full conversion, showing a maximum conversion of 67.3% and 65.2% at inlet CH_4 concentrations of 0.5 and 1 vol.% respectively.

On the other hand, it is worth mentioning the drop, and further recovery, in the catalytic activity due to the PdO-Pd-PdO phase transformation during the reactor cooling ramp, at around 550-600 °C, as also reported in several other studies on CH_4 oxidation over Pd-based catalyst [82–87]. Recently, we also reported a decrease in CH_4 conversion at medium/high temperatures when the PdO/CO_3O_4 catalyst amount coated on the single Zir OCF was varied [53]. The decrease in the catalytic activity was observed for all flow conditions studied (WHSV=30, 60, 90 and inlet CH_4 concentration of 0.5 and 1 vol. % [53]). Interestingly, in this work, when carrying out the catalytic CH_4 oxidation combining the coated SiCZir OCFs at the lowest WHSV of 30, the CH_4 conversion remains constant at 100% till very low temperature values, without being affected by the PdO-Pd-PdO phase transformation, except for the SiC2Zir1 combination at the inlet CH_4 concentration of 0.5 vol.%. However, as the WHSV increases to 90, the drop in the catalytic activity becomes evident in all OCF combinations, occurring at higher temperatures respect to the previous series of tests. Attractively, in terms of CH_4 conversion, the SiC1.5Zir1.5 combination showed the smallest performance drop due to the PdO-Pd-PdO phase transformation (from 100% to 90%) compared to the other foams combinations, even with those reported in our previous work at the same flow conditions on the coated Zir OCF [53]. Furthermore, it is important to note that at WHSV of 90, when the reactor operates with a higher CH_4 concentration and, hence, with a higher oxygen

concentration (O_2/CH_4 molar ratio constant and equal to 8), the shift of the curve is less accentuated (from 100% to 95%).

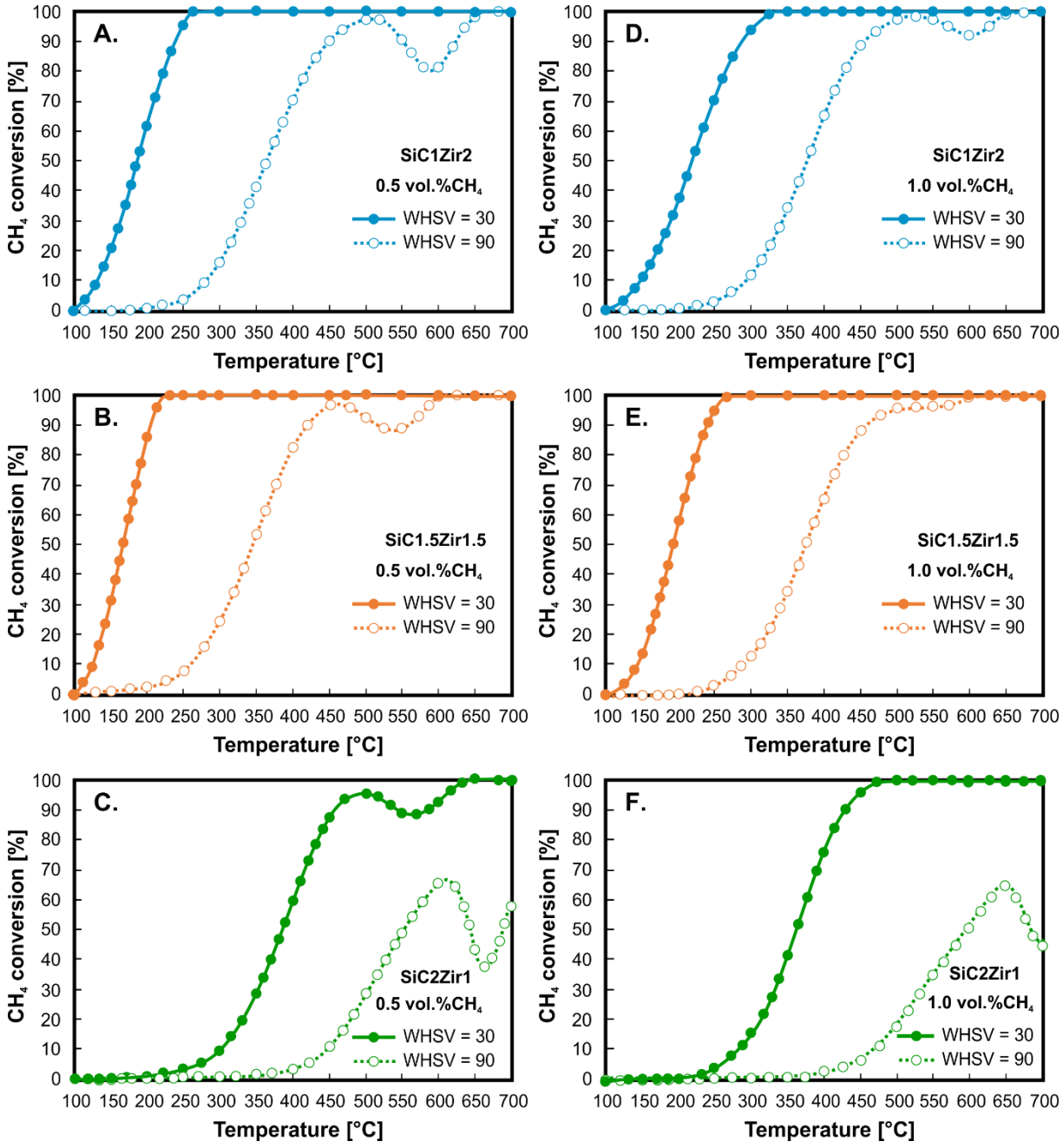

Figure 2. Extinction curves of CH_4 oxidation on 3 wt.% PdO/Co_3O_4 catalyst coated on SiC1Zir2 (A, D), SiC1.5Zir1.5 (B, E) and SiC2Zir1 (C, F) OCF combinations at WHSV of 30 and 90 NL h^{-1} g_{cat}^{-1} and intel CH_4 concentration of 0.5 and 1 vol.%.

Such a feature has also been reported in our previous work [53] and by other authors for highly exothermic reactions [57,59,87,88]. Various studies have pointed out that the increase in the partial pressure of O_2 favors the stabilization of the PdOx system by promoting the formation of PdO during the cooling phase (Pd ↔ PdO phase transformation) [29,83,86,87,89–92]. Farrauto et al. [93] also reported that as O_2 concentration increases, the hysteresis of the PdO-Pd-PdO phase transformation is shifted towards higher temperatures. Such an effect is also observed here, particularly during the catalytic tests performed at WHSV of 90 on the SiC2Zir1 combination (**Figures 2C and 2F**).

Figure 3 shows a comparison of the three coated SiCZir OCF combinations in terms of temperature at 10% (T_{10}) and 50% (T_{50}) methane conversion, for all flow conditions investigated. Specifically, when analyzing the shut-down temperature (T_{10}), the extinction of the reaction occurs at lower temperatures in the SiC1.5Zir1.5 and SiC1Zir2 combinations, showing a T_{10} difference between them below 15 °C at both WHSV and inlet CH_4 concentrations. On the other hand, the extinction for the SiC2Zir1 combination is anticipated, obtaining a T_{10} difference with respect to the SiC1.5Zir1.5 combination greater than 140 °C, at the same flow conditions. Regarding the T_{50}, at WHSV of 90, the SiC1Zir2 and SiC1.5Zir1.5 configurations exhibited similar values with a T_{50} difference below 15 °C. However, when operating the reactor at the lowest WHSV (30), the T_{50} difference between the latter increased to about 30 °C. Similar to the T_{10} results, the SiC2Zir1 combination showed the highest T_{50} values. Thus, according to the catalytic test results, it is possible to deduce that combining equal lengths of the coated SiC and Zir OCF pieces in the SiC1.5Zir1.5 configuration favors the catalytic performance of CH_4 oxidation, since it allows maintaining the reaction and the complete CH_4 conversion at lower temperatures. This result can be explained considering the difference in thermal conductivity of both foams. In fact, as we reported in our previous work [54], the volumetric heat transfer coefficient for the individual SiC OCF is about 25 times higher

than that of the Zir OCF. This could suggest a lower resistance to external heat transfer favoring the catalytic process.

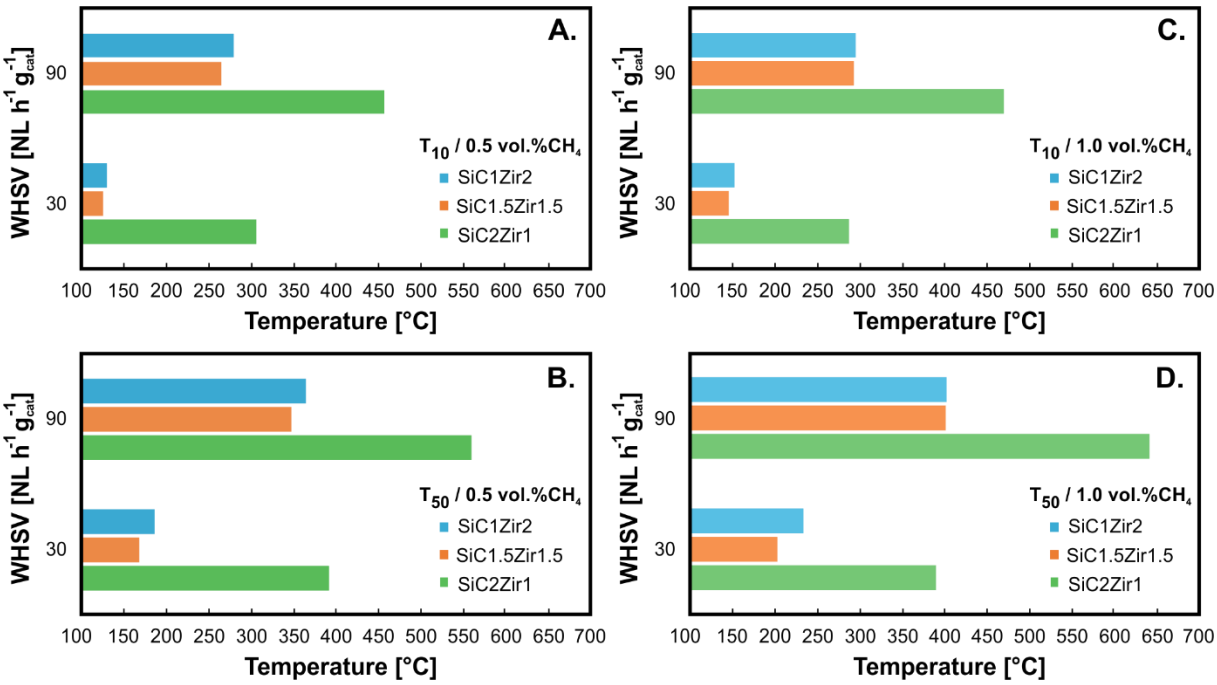

Figure 3. T_{10} and T_{50} of the three OCF combinations for all flow conditions studied during the extinction curves.

In order to highlight the effect on the catalytic performance towards CH_4 combustion in lean conditions when using different combinations of SiC and Zir OCFs, we compared the extinction curves of all the OCF combinations studied here with those obtained in our previous work on individual SiC and Zir OCFs [54], as shown in **Figure 4**. All of them were lined with 3 wt.% PdO/Co_3O_4 as catalyst and carried out at the same flow conditions (WHSV = 30 NL h^{-1} g_{cat}^{-1} and inlet CH_4 concentration of 0.5 vol.%).

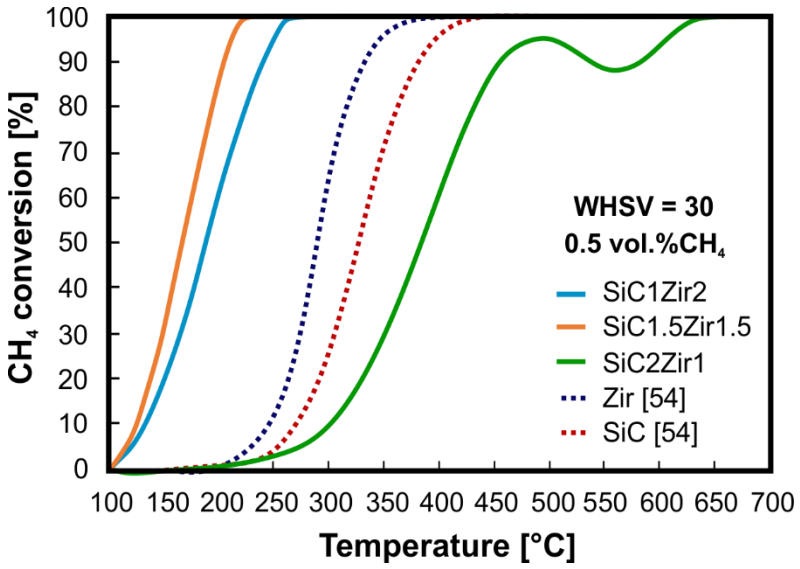

Figure 4. Extinction curves of CH_4 oxidation for 3 wt.% PdO/Co_3O_4 catalyst coated on individual SiC and Zir OCF (from our previous work Ercolino et al. [54]) and combinations of them at WHSV of 30 NL h^{-1} g_{cat}^{-1} and inlet CH_4 concentration of 0.5 vol.%.

Clearly, the SiC1Zir2 and SiC1.5Zir1.5 combinations offer a marked improvement in holding on the CH_4 conversion at low temperature. Particularly, the SiC1.5Zir1.5 combination allowed combustion extinction at 150 and 90 °C less than those obtained for the individual SiC and Zir OCFs, respectively. Furthermore, this OCF combination showed a decrease of the temperature of approximately 175 and 135 °C, with respect to the individual SiC and Zir OCFs. That is, the SiC1.5Zir1.5 combination maintained full CH_4 combustion till to the temperature of 215 °C (for 30 as WHSH and 0.5 vol.% as inlet CH_4 concentration), which is a remarkable result. This result shows a promising performance in heterogeneous catalysis for the complete oxidation of methane in lean conditions and at low temperature. Such outcome is of utmost importance especially for the intensification of processes where it is required to abate methane emissions at the lowest possible temperature [8–10].

3.2 Apparent kinetic parameters

Figure 5 shows the Arrhenius plot for all SiCZir OCF combinations studied at WHSV of 30 and inlet CH_4 concentration of 1 vol.%. The SiC2Zir1 combination curve shifts towards higher temperatures (lower 1/T values), indicating slower ignition of the reaction. On the other hand, the curves for the SiC1Zir2 and SiC1.5Zir1.5 configurations are quite close, with a slight shift towards lower temperatures for the SiC1.5Zir1.5 combination. The apparent activation energy (E_{app}) and the pre-exponential factor A_o were estimated at CH_4 conversions below 10 % to guarantee a kinetic regime in all structured catalysts (see **Table 2**). The kinetic parameters, also calculated for the three OCFs at WHSV of 90, were in line with the values obtained at the lower WHSV and with those we calculated for the 3% PdO/Co_3O_4 lined on single Zir and SiC foams in one of our previous paper (E_{app} = 85.9 kJ mol^{-1} for Zir, and 191.6 kJ mol^{-1} for SiC at WHSV 30, inlet CH_4 concentration 0.5% [52], instead of 1%).

Table 2. Apparent kinetic parameters estimated for the three OCF combinations at WHSV of 30 and 90 NL h^{-1} g_{cat}^{-1} and inlet CH_4 concentration of 1 vol.%

	30 WHSV (NL h^{-1} g_{cat}^{-1})		**90 WHSV (NL h^{-1} g_{cat}^{-1})**	
	E_{app} **(kJ mol^{-1})**	A_o **(m^3 g^{-1} s^{-1})**	E_{app} **(kJ mol^{-1})**	A_o **(m^3 g^{-1} s^{-1})**
SiC1Zir2	104.30	$3.78 \cdot 10^4$	96.30	$8.65 \cdot 10^3$
SiC1.5Zir1.5	102.42	$1.14 \cdot 10^7$	113.90	$8.03 \cdot 10^5$
SiC2Zir1	108.82	$1.68 \cdot 10^5$	109.06	$1.17 \cdot 10^2$

At higher temperature, the reaction rate increases and the reaction resistance decreases, thus the diffusional effects become important. This is observed in all the curves displayed in **Figure 5**, where it is possible to visualize the change in the slope ($-E_{app}/R_g$) of the Arrhenius plot as the temperature varies. At intermediate temperatures, a slope of about half compared to that obtained in the kinetic regime was found ($E_a^{id} \approx E_{app}/2$), evidencing the relevance of diffusional effects inside the catalyst. Finally, at very high temperatures the slope of the curve drops to a value close to zero, indicating the dominance of external diffusive effects ($E_a^{ed} \approx 0$).

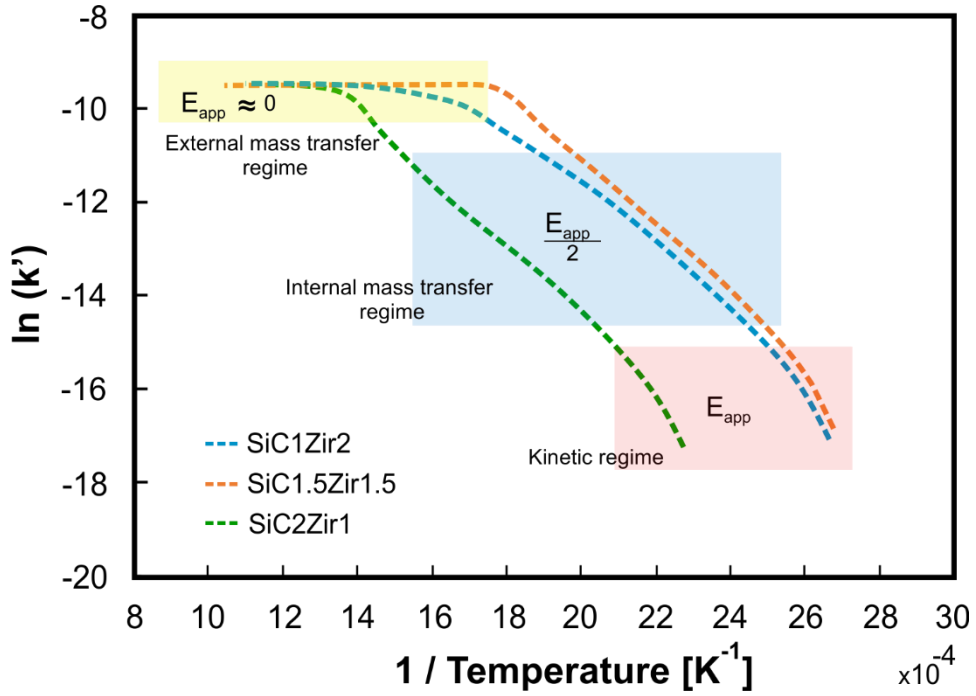

Figure 5. Arrhenius plots for the various OCF combinations (SiC1Zir2, SiC1.5Zir1.5, and SiC2Zir1) at WHSV of 30 and inlet CH_4 concentration of 1 wt.%.

3.3. External and internal mass transfer resistances

In **Figure 6**, the external (${R_m}^e$ or ${1/k_m}^e$) and internal (${R_m}^i$ or ${1/k_m}^i$) mass transfer resistances are plotted as a function of temperature at inlet CH_4 concentration of 1 vol.% and the two WHSV examined, for the three catalytic OCF combinations. At lower WHSV, SiC1Zir2 and SiC1.5Zir1.5 showed a dominance of ${R_m}^i$ at temperatures below ~400 °C (see **Figure 6A and**

6B). Thereafter, diffusional effects related to the fluid phase ($R_m{}^e$) start to become significant as the temperature continues to increase. For SiC2Zir1 the dominance of $R_m{}^i$ remains up to temperatures of approximately 690 °C, covering practically the entire temperature range studied (**Figure 6C**). On the other hand, with the increase of WHSV to 90, the external mass transfer coefficient increases as well, due to the enhancement of mixing (higher turbulence) in the gas phase. This leads to a remarkable decrease of the $R_m{}^e$, being irrelevant during almost the whole temperature range investigated and thus the $R_m{}^i$ becomes the crucial point for the catalyst performance. Both resistances show monotonic behavior with temperature, although the resistance to external mass transfer is almost independent of temperature.

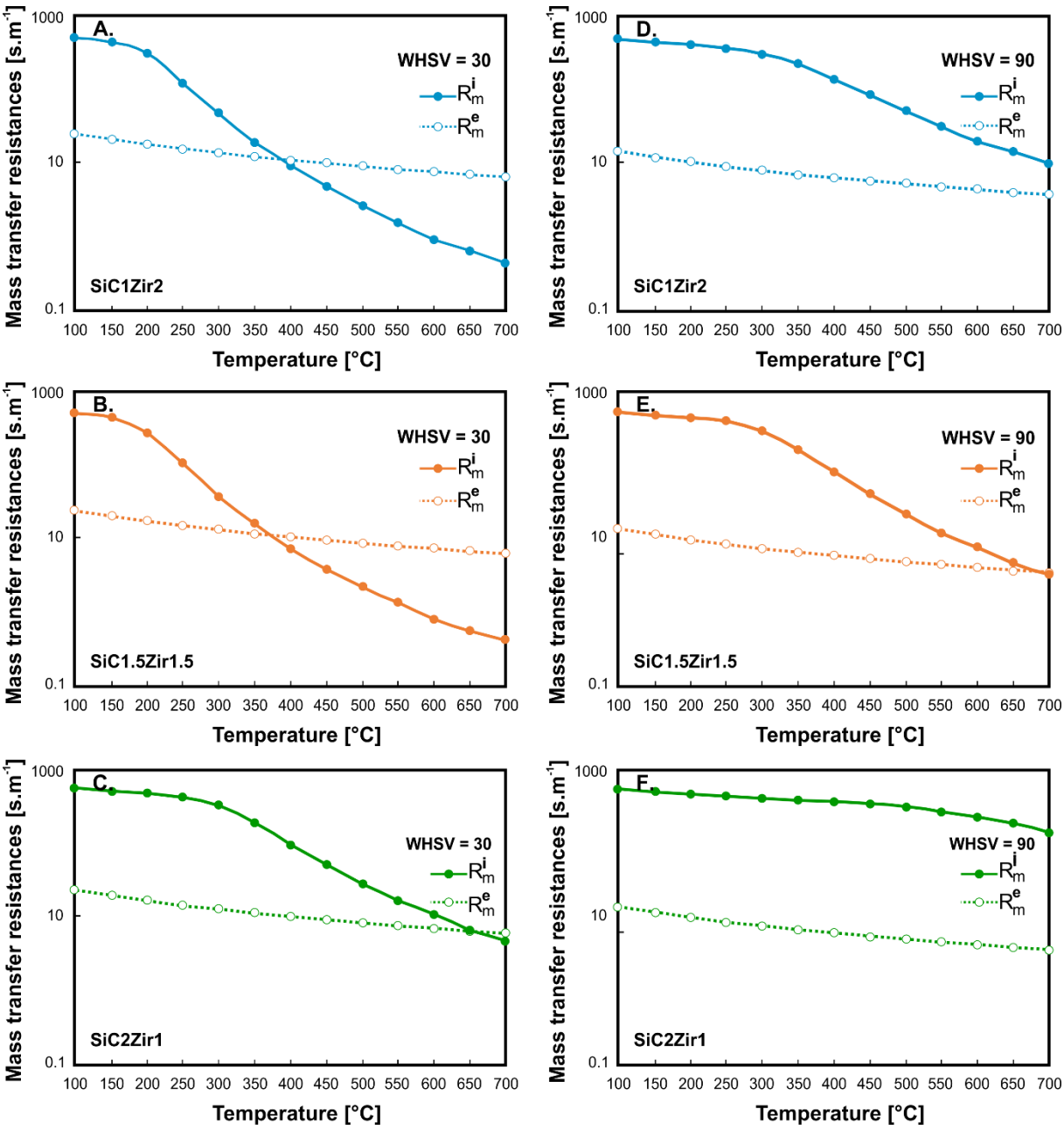

Figure 6. Mass transfer resistance as a function of temperature at inlet CH_4 concentrations of 1 vol.% and WHSV of 30 and 90 NL h^{-1} g_{cat}^{-1} for all OCF combinations: SiC1Zir2 (A, D); SiC1.5Zir1.5 (B, E) and SiC2Zir1 (C, F).

3.4. Overall catalytic performance: Kinetic and mass transfer regimes

We evaluated the operating regime (kinetic, internal and external mass transfer) of each SiCZir combination. For this purpose, we plotted the ratio of each resistance with respect to the total

resistance ($\frac{R_r}{R^{ov}}$; $\frac{{R_m}^i}{R^{ov}}$; $\frac{{R_m}^e}{R^{ov}}$) as a function of gas temperature, at WHSV of 30 and 90 and inlet CH_4 concentration of 1 vol.%, as shown in **Figure 7**.

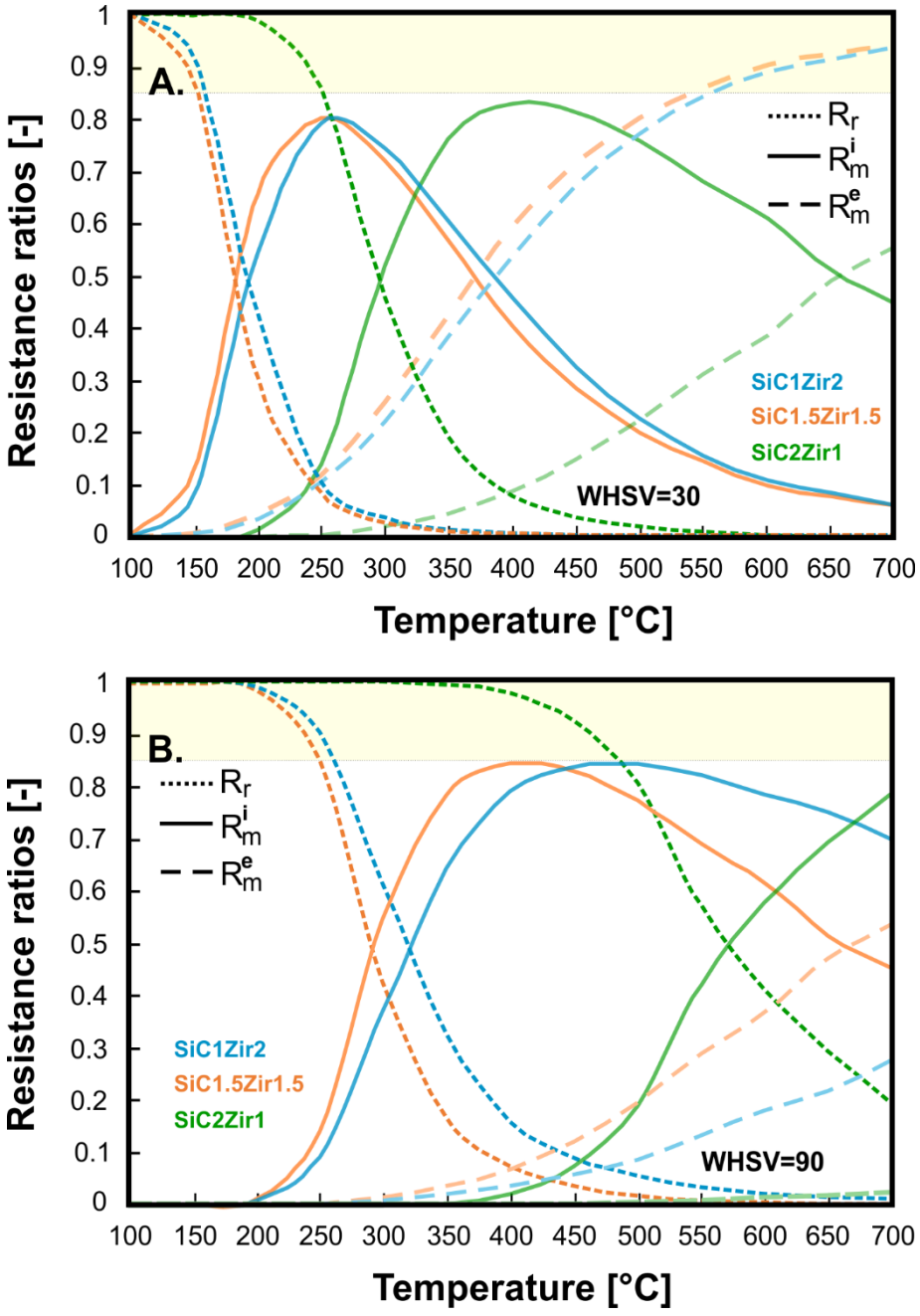

Figure 7. Various resistance ratios as a function of temperature showing the different operating regimes for the three OCF combinations at inlet CH_4 concentration of 1 vol. % and WHSV of 30 (A) and 90 (B) NL h^{-1} g_{cat}^{-1}.

As a general trend, the increase of temperature leads to a sharp drop of the $\frac{R_r}{R^{ov}}$ ratio due to the increase of the reaction rate, which is strongly dependent on the Arrhenius equation. On the other hand, as the temperature increases, the $\frac{{R_m}^i}{R^{ov}}$ ratio progressively increases (the intra-particle effects become more and more significant), reaching a maximum value, for then decreasing gradually with temperature. As for the external diffusional effects, the $\frac{{R_m}^e}{R^{ov}}$ ratio shows a progressive increase with increasing temperature, becoming much more significant at lower WHSV and very high temperatures.

When analyzing the operating regimes at WHSV of 30 (see **Figure 7A**), at temperatures below 148, 160, and 255 °C for SiC1.5Zir1.5, SiC1Zir2 and SiC2Zir1, respectively, the reaction kinetics dominates the process ($\frac{R_r}{R^{ov}} > 0.85$), being the reaction resistance controlling, thus the catalyst operates in a kinetic regime. As the temperature increases, the reaction rate becomes increasingly faster, thus internal diffusion effects start to become significant. In particular, at temperatures between 180-370 °C, 190-395 °C and 295-660 °C the diffusion inside the PdO/Co_3O_4 layer becomes the pivotal resistance of the catalytic process for the OCF combinations of SiC1.5Zir1.5, SiC1Zir2 and SiC2Zir1, respectively. However, considering that by convention a reaction is defined under internal resistance control regime for a thresold limit value of 85% [71,72], in our case the structured catalysts cannot be considered under internal resistance control (all the curves show a $\frac{{R_m}^i}{R^{ov}} < 0.85$). On the other hand, only the coated SiC1Zir2 and SiC1.5Zir1.5 structures exhibit an external diffusive regime at temperature above roughly 550 °C.

When operating the reactor at the higher WHSV (see **Figure 7B**), the kinetic regime ($\frac{R_r}{R^{ov}} > 0.85$) shifts towards higher temperatures, due to the shorter contact time. Specifically, at temperatures below 250, 260, and 485 °C the catalyst operates in the kinetic regime for OCF combinations of SiC1.5Zir1.5, SiC1Zir2 and SiC2Zir1, respectively. As mentioned above, the

increase in gas velocity produces an enhancement of mixing and thus an increase of the external mass transfer coefficient. In this way, the dominant resistance at medium-high temperatures becomes the ${R_m}^i$. Nevertheless, the $\frac{{R_m}^i}{R^{ov}}$ ratios are not higher than 0.85 to be considered as a controlling regime. Therefore, once the kinetic control is overcome (as the temperature increases), the catalyst operates in a mixture of regimes where R_r and ${R_m}^i$ are comparable at low/medium temperatures, while ${R_m}^i$ and ${R_m}^e$ at medium/high temperatures.

For further analysis, we plotted the effectiveness factor, η (**Figure 8B**) and the evolution of R_r and ${R_m}^i$ (**Figure 8A**) as a function of the Thiele modulus (ϕ) at WHSV of 30 and 1 vol.% as inlet CH_4 concentration. Clearly, in the case of very slow reactions, the $\phi \ll 1$ and the $\eta \to 1$. At this point, the R_r controls the catalytic combustion and ${R_m}^i$ tends to the asymptotic value of $\frac{R_{\Omega,i}}{Sh_{c,\infty} \cdot D_e}$, being independent of the reaction kinetics and catalytic thickness dependent [71]. On the contrary, in the limit of very fast reactions (for $\phi \gg 1$; $\eta \to \frac{1}{\phi}$), the R_r is negligible and thus, the diffusional effects control the process, where the ${R_m}^i$ tends to the value of $\frac{1}{\sqrt{k \cdot D_e}}$ [72]. Therefore, the ${R_m}^i$ is independent of the catalytic thickness and depends only on the combustion kinetics and the effective diffusivity inside the catalyst [40,63,72,73,94].

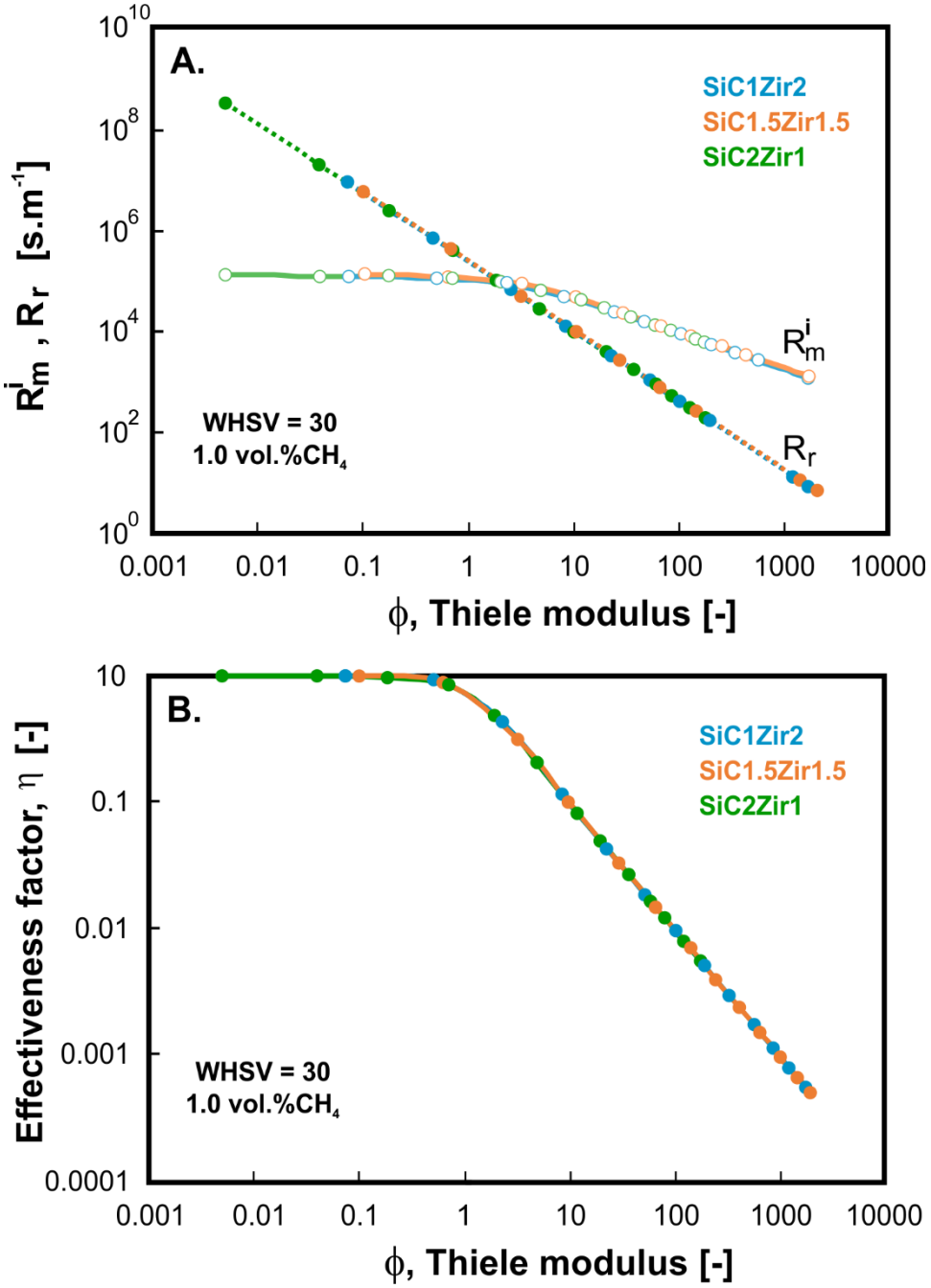

Figure 8. Evolution of R_r and $R_m{}^i$ (A) and effectiveness factor (B) as a function of the Thiele modulus (ϕ) at WHSV of 30 and inlet CH_4 concentration of 1 vol.%.

3.5. External and internal heat transfer evaluation

Figure 9 shows the Nusselt number and volumetric heat transfer coefficient as a function of Reynolds number defined at temperatures of 200, 400, and 600 °C for the three OCF combinations and for each individual SiC and Zir OCF reported in our previous work [54].

Clearly, the higher the gas velocity, the greater the fluid turbulence in the foam flow paths, and hence the convective heat transfer increases. At the same flow conditions, the gas surface velocity is higher with increasing SiC OCF length in the combinations. This is because the SiC OCF has a lower average pore diameter value [61], thus as the SiC OCF length increases in each combination, more of the reactive flow passes through the entire configuration at a higher velocity. Examining the effect of temperature, at 200 °C higher Nu values are obtained by increasing the length of the SiC OCF (SiC2Zir1 > SiC1.5Zir1.5 > SiC1Zir2). However, increasing the temperature up to 600 °C led to very similar Nu values for all OCF combinations, due to the decrease in viscosity of the reactive mixture. These effects play a key role in the volumetric heat transfer coefficients, which, at same flow conditions are higher for the combinations with longer SiC foam length, thanks to the higher thermal conductivity that they offer compared to Zir OCF. Thus, by combining SiCZir OCFs a remarkable increase of the volumetric heat transfer coefficient is obtained. The h_e^v values are in line with those reported by Dietrich [95] and Xia et. al [96] for OCFs, and also other reactor configurations, such as packed bed reactors and monoliths [45,97–99].

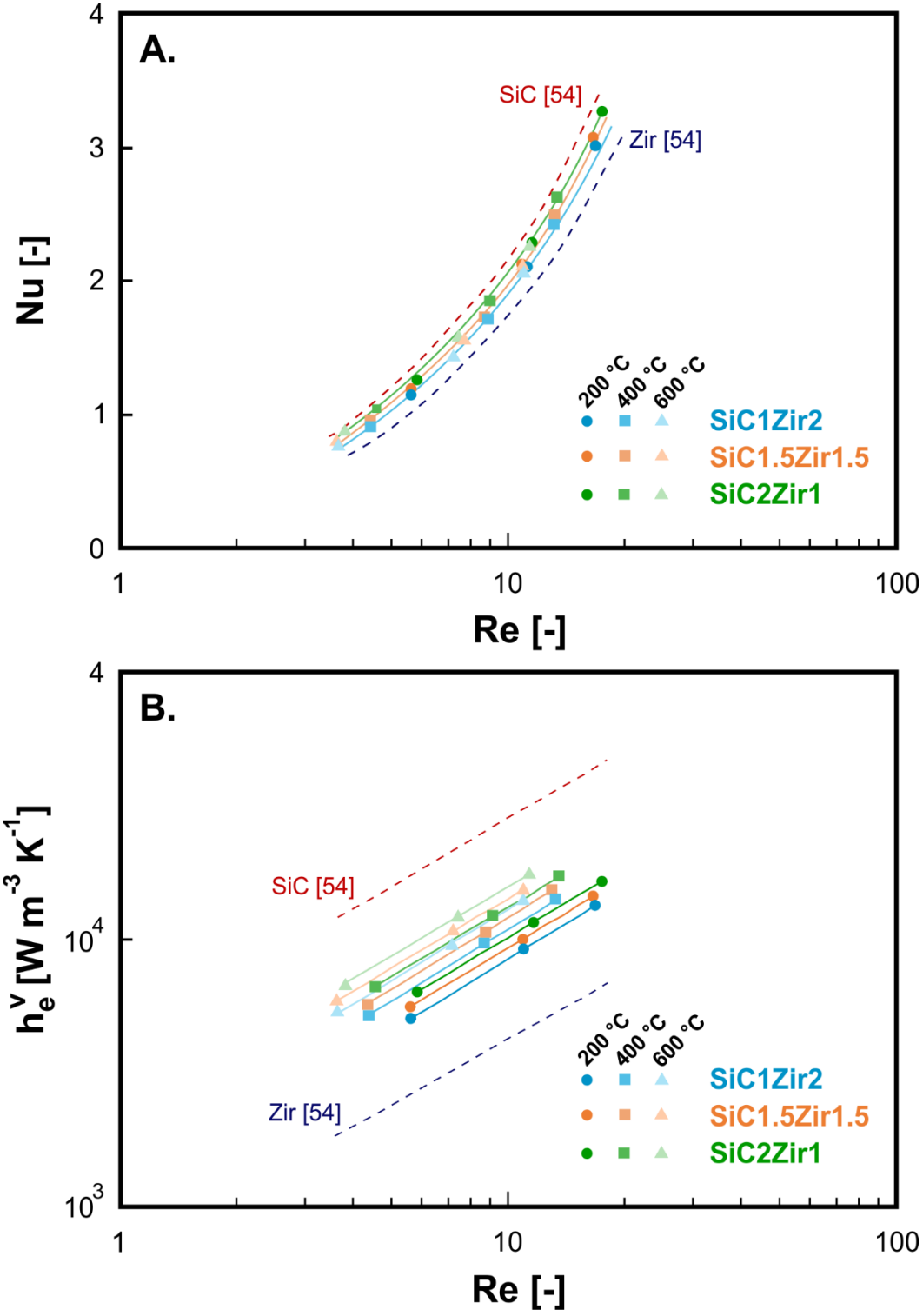

Figure 9. Nusselt number (A) and volumetric heat transfer coefficient (B) as a function of Reynolds number defined at temperatures of 200, 400, and 600 °C for the three OCF combinations and for each individual SiC and Zir OCF reported in our previous work [54].

To evaluate the effects of external heat transfer in all SiCZir OCF combinations, we used the Mears criterion according to **Equation 18**, for both WHSV studied and inlet CH_4 concentration of 1 vol.%.

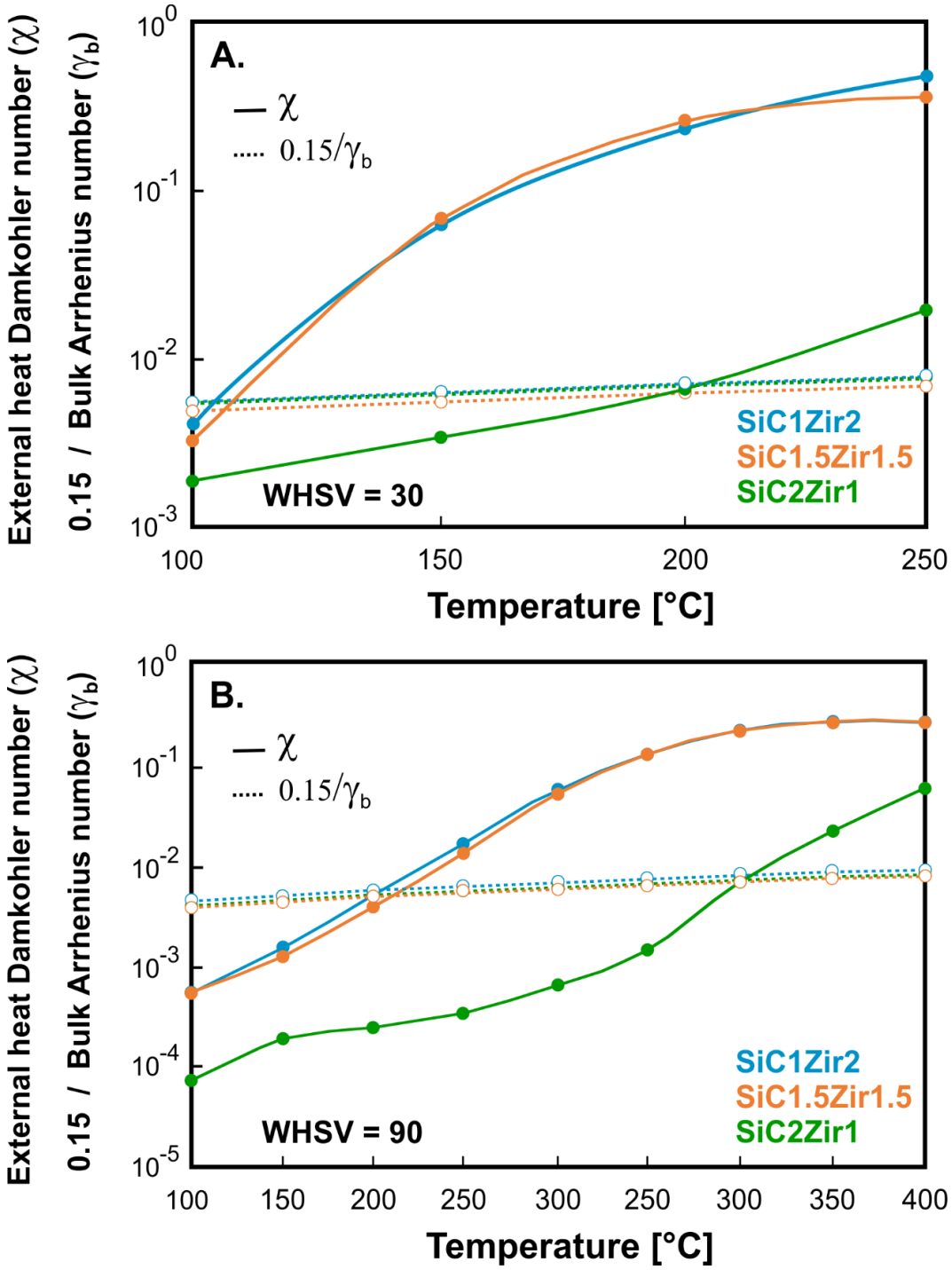

Figure 10. Mears criterion to evaluate external heat transfer for all OCF combinations at inlet CH_4 concentration of 1 vol.% and WHSV of 30 (A) and 90 (B).

At lower reactive gas flow and hence low WHSV (**Figure 10A**), external heat transfer limitations are present at higher temperatures of 105, 115, and 200 °C for the combinations of SiC1Zir2, SiC1.5Zir1.5, and SiC2Zir1, respectively. On the other hand, by increasing the WHSV to 90, a higher gas turbulence is obtained and hence higher heat transfer coefficients (**Figure 9**), which leads to shift the external heat transfer limitations to higher temperatures, as shown in **Figure 10B**. Such limitations could be due to the rapid ignition of the reaction, which results in a higher heat production due to the exothermicity of the combustion process, with respect to the heat removed by the flue gases. By analyzing the heats of removal (Q) and reaction (Q_r) as a function of temperature at the two WHSV and inlet CH_4 concentration of 1 vol.% (see **Figure 11**), the SiC1Zir2 and SiC1.5Zir1.5 combinations show similar values of Q_r and Q (at both space velocities), with slightly higher values for SiC1.5Zir1.5. In particular, the latter exhibits a $Q > Q_r$ (stable operating zone) at lower temperatures of 160 and 272 °C at WHSV of 30 and 90, respectively. In contrast, the SiC2Zir configuration displays the lowest Q and Q_r when compared to the other combinations, operating in a stable zone at temperatures below 230 and 650 °C at WHSV of 30 and 90 NL h^{-1} g_{cat}^{-1}, respectively. Once the catalyst reaches conversions above 90 % (**Figure 2**), that is, when the reaction rate constant is sufficiently high and hence the R_r is negligible ($R_r \ll {R_m}^e + {R_m}^i$), the heat removal becomes stable reaching similar values at elevated temperatures for the three OCF combinations.

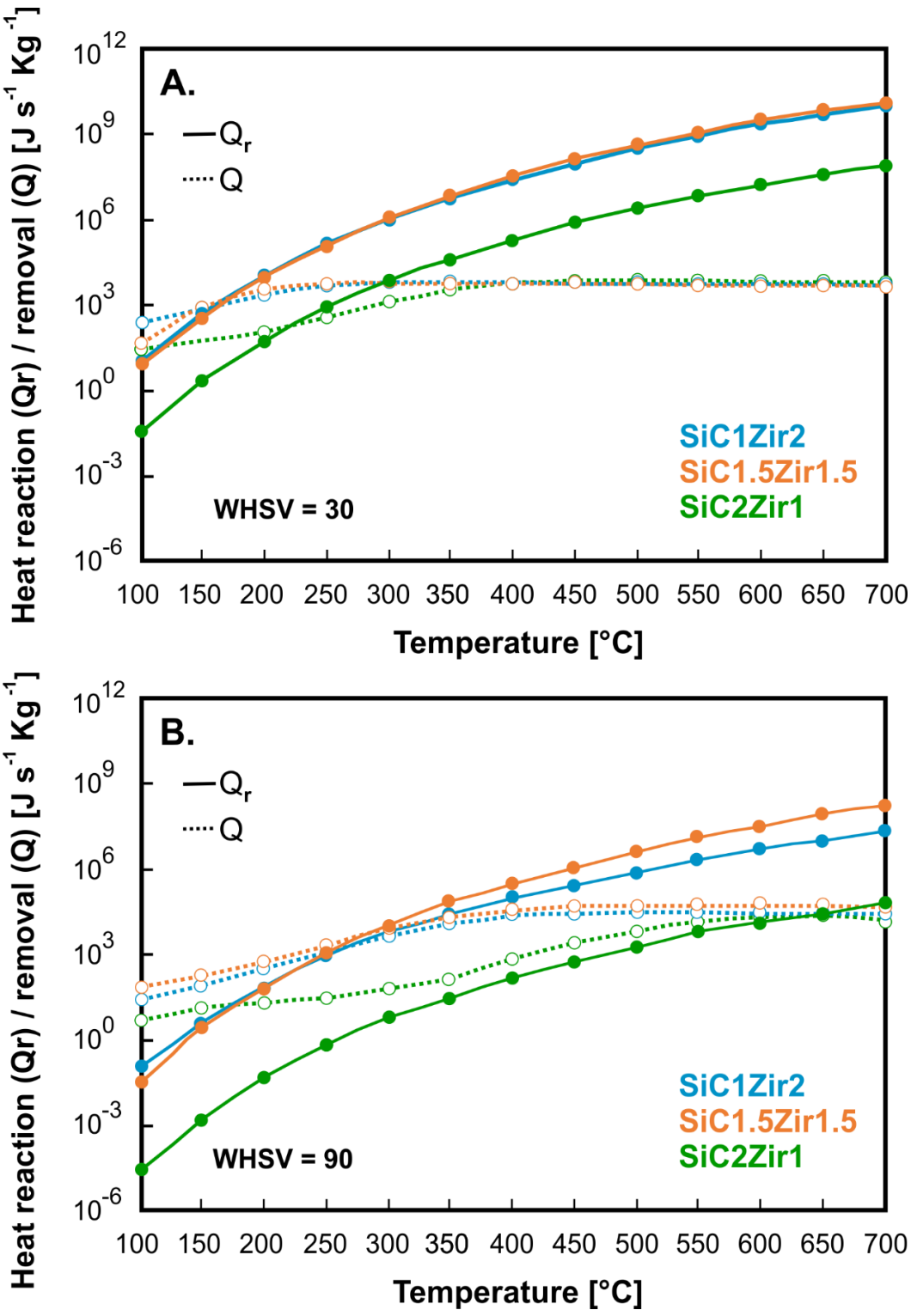

Figure 11. Heat reaction and removal rates as a function of bulk temperature for all the OCF combinations at WHSV of 30 (A) and 90 (B) and inlet CH_4 concentration of 1 vol.%

The presence of SiC OCF at the inlet of the reactor, which has a higher thermal conductivity compared to Zir OCF, is helpful to retain the heat of reaction for boosting the ignition of the first reacting molecules on the surface of the catalyst at low temperature during the heating ramp, and to hold the reaction on during the cooling ramp of the tests [54,99]. The optimal configuration is reached in the SiC1.5Zir1.5 combination, where the kinetics and thermal effects of the two foams are synergetically enhanced by combining two supports with different thermal conductivity but equal lenght. The OCF in front, with a higher thermal conductivity, to boost the ignition of the catalytic reaction at low temperature, the following one with a lower thermal conductivity, to reach and maintain full combustion at the lowest possible temperature. For further analysis, we plotted the temperature difference between the bulk gas phase and the external catalyst surface (according to **Equation 27**) as a function of temperature for all the conditions examined (**Figure 12**). This is a purely qualitatively analysis since the T_s is a theoretical average temperature calculated taking into account the different properties of the two OCFs and their relative lengths, and it does not represent any real surface temperature. Moreover, in the tests we made on single OCFs [54], we measured a temperature gradient between the inlet and outlet of the foams, being the $\Delta(T_{in} - T_{out})$ values of the Zir foams very limited, representative of an isothernal system, while the $\Delta(T_{in} - T_{out})$ values of the SiC slightly more positive, representative of a quasi-isothermal system, at various temperatures and WHSV. Consequently, in our SiCZir configurations we expect inlet/outlet temperature gradients. Thus, the following considerations are purely speculative, but helpful in understanding what is happening in the catalytic systems during reaction.

As observed from our calculations, the increase in CH_4 concentration leads to a higher adiabatic temperature (ΔT_{ad}) in the catalytic system and thus a greater $(T_s - T_b)$. The temperature difference increases rapidly until the catalyst reaches full CH_4 conversion. At this point the $(T_s - T_b)$ starts to decay gradually as the gas temperature increases. The highest temperature

difference was found for the SiC1.5Zir1.5 combination for all flow conditions studied. A greater $(T_s - T_b)$, that is a higher T_s, should hold the combustion reaction, thus exploiting the extinction temperature at lower values. However, at higher WHSV, the contact times decreases, and the Carberry values increases with temperature, reaching a maximum values approaching full methane conversion, thus shifting the extinction temperature to greater values. This is also visible by the significative increase of the diffusional effects related to the fluid phase as the temperature raises, as visible from **Figure 6.** These two effects combined together prevail on the advantage of a greater $(T_s - T_b)$, with the consequence that at higher WHSV and higher CH_4 inlet concentration, the combustion reaction worsen.

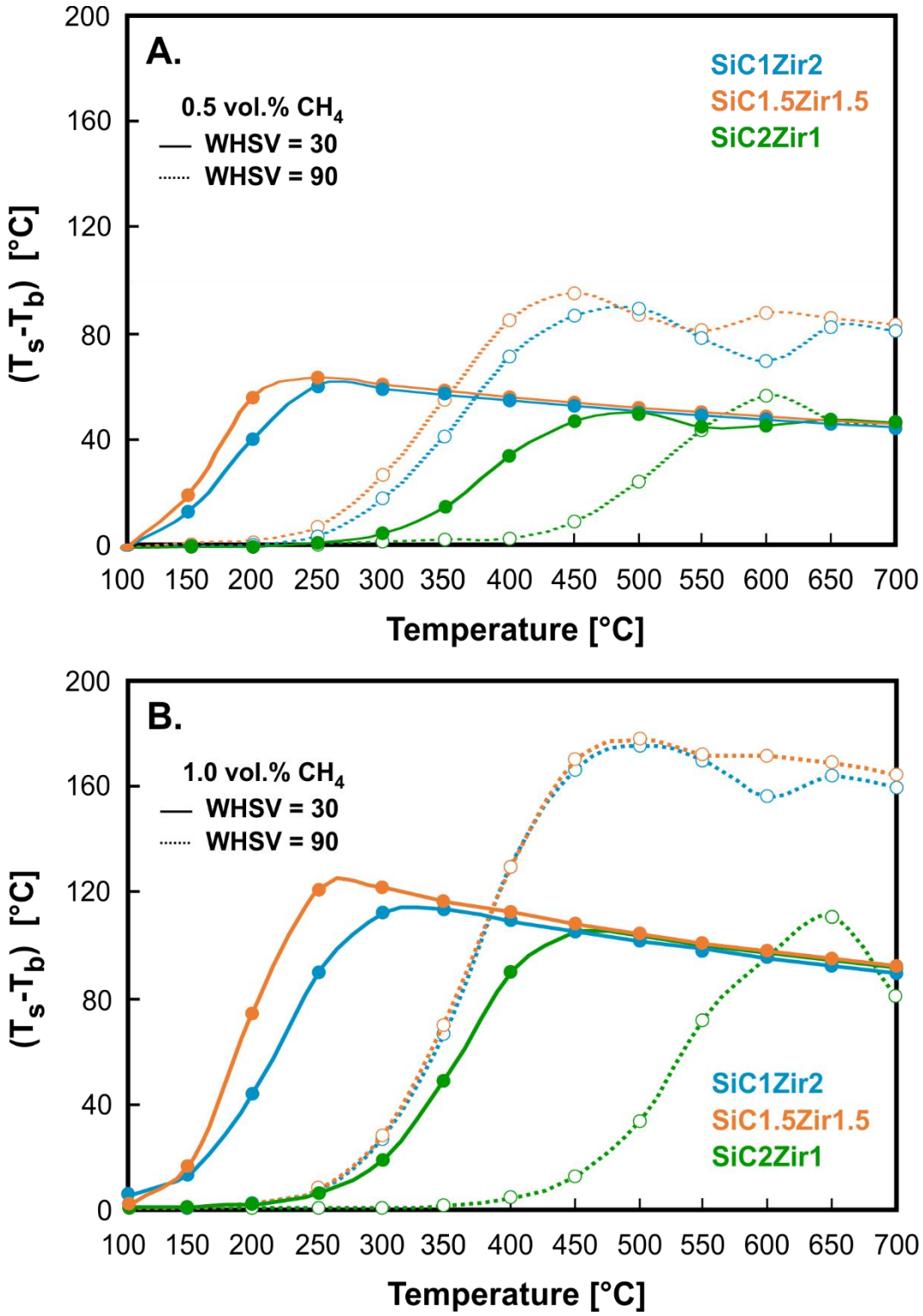

Figure 12. Temperature difference between the bulk gas phase and the external catalyst surface as a function of temperature at WHSV of 30 and 90 and inlet CH_4 concentration of 0.5 (A) and 1 vol.% (B) for all the OCF combinations investigated.

Regarding internal heat transfer, we plotted in **Figure 13** the Anderson criterion for all OCF combinations at inlet CH_4 concentrations of 1 vol.% and the two WHSV. No heat limitations were found within the catalyst layer thickness, indicating the absence of intraparticle temperature gradients in all OCF configurations.

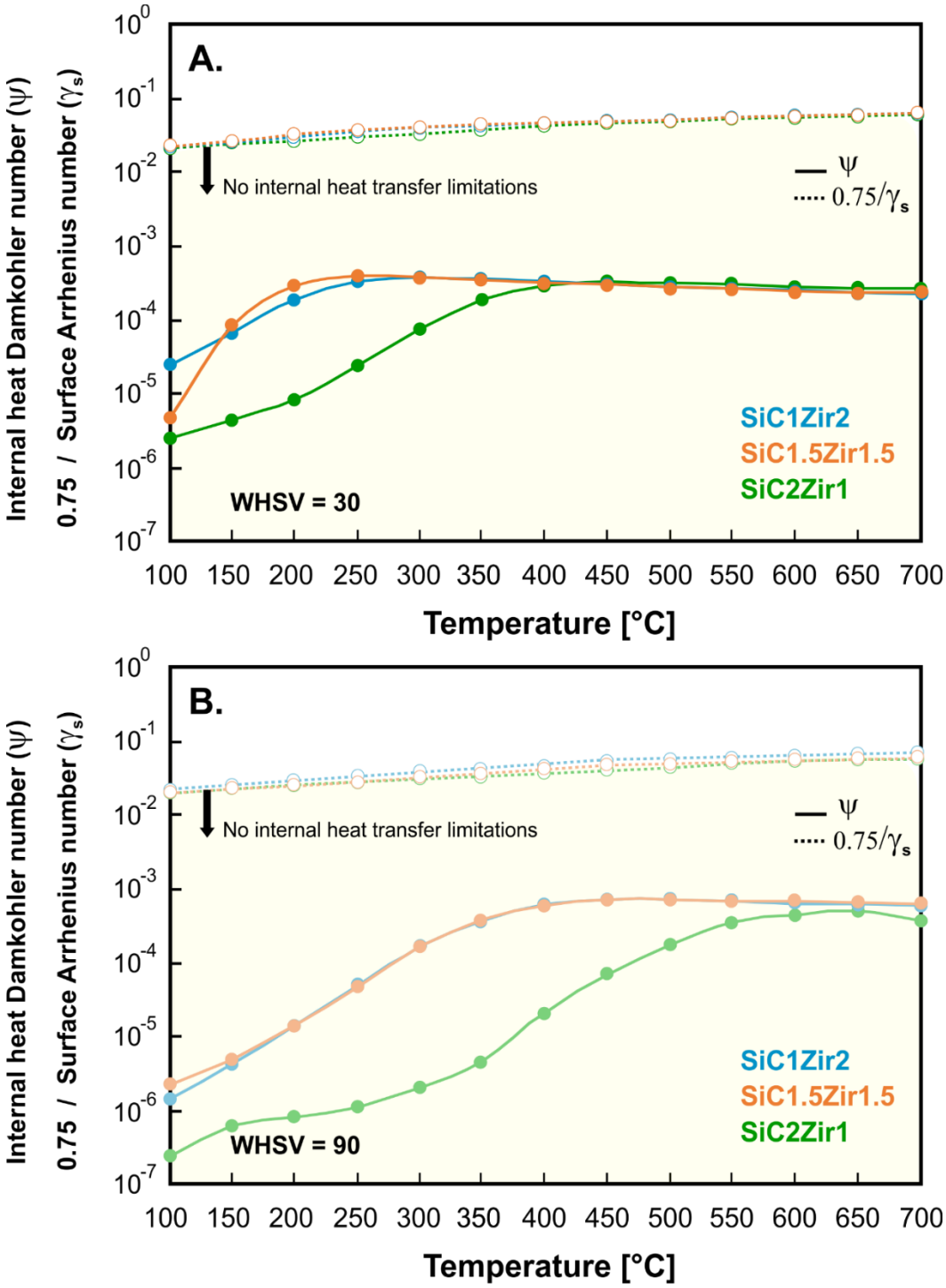

Figure 13. Anderson criterion to evaluate internal heat transfer for all OCF combinations at inlet CH_4 concentration of 1 vol.% and WHSV of 30 (A) and 90 (B).

5. Conclusions

The main contribution of this work is to evaluate the catalytic performance towards complete CH_4 combustion in lean conditions by using three different OCF combinations made of SiC and Zir with pore densities of 30 ppi coated with 3 wt. % PdO/Co_3O_4 as catalyst. The reactor feed was carried out in a large excess of oxygen (O_2/ CH_4 molar ratio equal to 8), with inlet CH_4 concentrations of 0.5 and 1 vol. % and WHSV of 30 and 90 NL h^{-1} g_{cat}^{-1}. The apparent kinetic parameters of the structured catalysts were determined in order to estimate the reaction resistance. In addition, external and internal mass transfer effects were evaluated using a theoretical model adapted to the OCF geometry, which allowed the determination of the mass transport resistances. The operating regime of each OCF combination was determined by varying the temperature of the reactive gas. Furthermore, an analysis of heat transfer effects was carried out in terms of volumetric heat transfer coefficients, possible heat limitations using theoretical criteria (Mears and Anderson criteria), heats of removal and reaction, and theoretical evaluation of the temperature difference between the gas bulk and the external catalyst surface. The following major conclusions can be drawn from this study:

- Among the three foam combinations, SiC1.5Zir1.5 exhibited complete methane conversion at the lowest temperatures for all flow conditions studied.
- The remarkable catalytic performance of the SiC1.5Zir1.5 configuration, which maintained full methane conversion at the lowest extinction temperature of 215 °C (WHSV of 30 and 0.5 vol.% as inlet CH_4 concentration), can be explained considering the different thermal conductivity of the SiC and Zir used as supports for the PdO/Co_3O_4 catalyst. The presence of SiC OCF at the inlet of the reactor, which has a higher thermal

conductivity compared to that of Zir OCF, is helpful to hold on the heat of reaction, thus shifting the extinction temperature at lower values. The optimal configuration is reached in the SiC1.5Zir1.5 system combination, where two supports of same length but with different thermal conductivity are used in series. With such a configuration, we reached a favorable balance of heat and mass transfers acting synergistically to drive and hold the combustion reaction even at low temperature.

- The temperature difference between the bulk of the fluid phase and the external catalyst surface increases rapidly in the combinations with faster ignition of the reaction, until the catalyst reaches near full conversion and then gradually decreases as the gas temperature increases.
- The mass transport limitations, ignition/extinction behavior, and presence of multiple steady-state conditions of a catalytic system are of utmost importance to design new compact catalytic reactors for process intensification of highly exothermic reactions.

CRediT author statement

C.W. Moncada Quintero: Conceptualization, Methodology, Investigation, Data curation, Formal analysis, Validation, Writing - original draft, Writing - review & editing. G. Ercolino: Conceptualization, Investigation, Data curation. S. Specchia: Conceptualization, Methodology, Validation, Supervision, Writing - review & editing, Funding acquisition, Resources.

Declaration of Competing Interest

The authors report no declarations of interest.

Acknowledgements

This work was supported by the Italian Ministry of Education, University and Research (MIUR, Italy), via the ERANETMED network (SOLCARE project, grant number ENERG-065).

References

[1] Understanding Global Warming Potentials | Greenhouse Gas (GHG) Emissions | US EPA, (n.d.). https://www.epa.gov/ghgemissions/understanding-global-warming-potentials.

[2] E.J. Dlugokencky, E.G. Nisbet, R. Fisher, D. Lowry, Global atmospheric methane: Budget, changes and dangers, Philos. Trans. R. Soc. A Math. Phys. Eng. Sci. 369 (2011) 2058–2072. https://doi.org/10.1098/rsta.2010.0341.

[3] IPCC, Climate Change 2014 Part A: Global and Sectoral Aspects, 2014. papers2://publication/uuid/B8BF5043-C873-4AFD-97F9-A630782E590D.

[4] R.K. Pachauri, L. Meyer, Climate Change 2014: Synthesis Report. Contribution of Working Groups I, II and III to the Fifth Assessment Report of the Intergovernmental Panel on Climate Change, IPCC, Geneva, Switzerland, 2014.

[5] E.J. Dlugokencky, Global Monitoring Laboratory - Carbon Cycle Greenhouse Gases, US Dep. Commer. NOAA, Glob. Monit. Lab. (2019). https://www.esrl.noaa.gov/gmd/ccgg/trends_ch4/ (accessed September 28, 2020).

[6] Global Methane Initiative, Global methane emissions by sector, 2020 (2010) 1–4. www.globalmethane.org.

[7] Methane Tracker 2020 – Analysis - IEA, (n.d.). https://www.iea.org/reports/methane-tracker-2020.

[8] J.K. Stolaroff, S. Bhattacharyya, C.A. Smith, W.L. Bourcier, P.J. Cameron-Smith, R.D. Aines, Review of methane mitigation technologies with application to rapid release of methane from the arctic, Environ. Sci. Technol. 46 (2012) 6455–6469.

https://doi.org/10.1021/es204686w.

[9] P. Gélin, L. Urfels, M. Primet, E. Tena, Complete oxidation of methane at low temperature over Pt and Pd catalysts for the abatement of lean-burn natural gas fuelled vehicles emissions: Influence of water and sulphur containing compounds, Catal. Today. 83 (2003) 45–57. https://doi.org/10.1016/S0920-5861(03)00215-3.

[10] I. Karakurt, G. Aydin, K. Aydiner, Mine ventilation air methane as a sustainable energy source, Renew. Sustain. Energy Rev. 15 (2011) 1042–1049. https://doi.org/10.1016/j.rser.2010.11.030.

[11] N.M. Kinnunen, J.T. Hirvi, M. Suvanto, T.A. Pakkanen, Methane combustion activity of Pd–PdO_x–Pt/Al_2O_3 catalyst: The role of platinum promoter, J. Mol. Catal. A Chem. 356 (2012) 20–28. https://doi.org/10.1016/j.molcata.2011.12.023.

[12] W.R. Schwartz, L.D. Pfefferle, Combustion of methane over palladium-based catalysts: Support interactions, J. Phys. Chem. C. 116 (2012) 8571–8578. https://doi.org/10.1021/jp2119668.

[13] M. Monai, T. Montini, R.J. Gorte, P. Fornasiero, Catalytic Oxidation of Methane: Pd and Beyond, Eur. J. Inorg. Chem. 2018 (2018) 2884–2893. https://doi.org/10.1002/ejic.201800326.

[14] H. Stotz, L. Maier, A. Boubnov, A.T. Gremminger, J.D. Grunwaldt, O. Deutschmann, Surface reaction kinetics of methane oxidation over PdO, J. Catal. 370 (2019) 152–175. https://doi.org/10.1016/j.jcat.2018.12.007.

[15] G. Ercolino, P. Stelmachowski, G. Grzybek, A. Kotarba, S. Specchia, Optimization of Pd catalysts supported on Co_3O_4 for low-temperature lean combustion of residual methane, Appl. Catal. B Environ. 206 (2017) 712–725. https://doi.org/10.1016/j.apcatb.2017.01.055.

[16] L.F. Liotta, G. Di Carlo, G. Pantaleo, G. Deganello, Catalytic performance of

Co_3O_4/CeO_2 and $Co_3O_4/CeO_2–ZrO_2$ composite oxides for methane combustion: Influence of catalyst pretreatment temperature and oxygen concentration in the reaction mixture, Appl. Catal. B Environ. 70 (2007) 314–322. https://doi.org/10.1016/j.apcatb.2005.12.023.

[17] M.M. Fiuk, A. Adamski, Activity of $MnO_x–CeO_2$ catalysts in combustion of low concentrated methane, Catal. Today. 257 (2015) 131–135. https://doi.org/10.1016/j.cattod.2015.01.029.

[18] G. Ercolino, P. Stelmachowski, A. Kotarba, S. Specchia, Reactivity of Mixed Iron–Cobalt Spinels in the Lean Methane Combustion, Top. Catal. 60 (2017) 1370–1379. https://doi.org/10.1007/s11244-017-0826-9.

[19] S. Specchia, A. Civera, G. Saracco, V. Specchia, Palladium/perovskite/zirconia catalytic premixed fiber burners for efficient and clean natural gas combustion, Catal. Today. 117 (2006) 427–432. https://doi.org/10.1016/j.cattod.2006.06.041.

[20] N. Miniajluk, J. Trawczyński, M. Zawadzki, P.E. Tomaszewski, W. Mišta, Solvothermal synthesis and characterization of mixed oxides with perovskite-like structure, Catal. Today. 257 (2015) 26–34. https://doi.org/10.1016/j.cattod.2015.03.029.

[21] Z. Ren, V. Botu, S. Wang, Y. Meng, W. Song, Y. Guo, R. Ramprasad, S.L. Suib, P.-X. Gao, Monolithically Integrated Spinel $M_xCo_{3–x}O_4$ (M=Co, Ni, Zn) Nanoarray Catalysts: Scalable Synthesis and Cation Manipulation for Tunable Low-Temperature CH_4 and CO Oxidation, Angew. Chemie. 126 (2014) 7351–7355. https://doi.org/10.1002/ange.201403461.

[22] A.M. Venezia, V. La Parola, L.F. Liotta, Structural and surface properties of heterogeneous catalysts: Nature of the oxide carrier and supported particle size effects, Catal. Today. 285 (2017) 114–124. https://doi.org/10.1016/j.cattod.2016.11.004.

[23] U. Zavyalova, P. Scholz, B. Ondruschka, Influence of cobalt precursor and fuels on the performance of combustion synthesized Co_3O_4/γ-Al_2O_3 catalysts for total oxidation of methane, Appl. Catal. A Gen. 323 (2007) 226–233. https://doi.org/10.1016/j.apcata.2007.02.021.

[24] M. Verelst, T.O. Ely, C. Amiens, E. Snoeck, P. Lecante, A. Mosset, M. Respaud, J.M. Broto, B. Chaudret, Synthesis and Characterization of CoO, Co_3O_4, and Mixed Co/CoO Nanoparticules, 11 (1999) 2702–2708. https://doi.org/10.1021/cm991003h.

[25] E. Barrera, I. González, T. Viveros, A new cobalt oxide electrodeposit bath for solar absorbers, Sol. Energy Mater. Sol. Cells. 51 (1998) 69–82. https://doi.org/10.1016/S0927-0248(97)00209-2.

[26] S. Weichel, P.J. Møller, Annealing-induced microfaceting of the CoO(100) surface investigated by LEED and STM, Surf. Sci. 399 (1998) 219–224. https://doi.org/10.1016/S0039-6028(97)00820-0.

[27] F. Švegl, B. Orel, M.G. Hutchins, K. Kalcher, Structural and Spectroelectrochemical Investigations of Sol-Gel Derived Electrochromic Spinel Co_3O_4 Films, J. Electrochem. Soc. 143 (1996) 1532–1539. https://doi.org/10.1149/1.1836675.

[28] G.B. Hoflund, Z. Li, Surface characterization study of a Pd/Co_3O_4 methane oxidation catalyst, Appl. Surf. Sci. 253 (2006) 2830–2834. https://doi.org/10.1016/j.apsusc.2006.05.115.

[29] D. Ciuparu, E. Altman, L. Pfefferle, Contributions of lattice oxygen in methane combustion over PdO-based catalysts, J. Catal. 203 (2001) 64–74. https://doi.org/10.1006/jcat.2001.3331.

[30] J. Votruba, J. Sinkule, V. Hlaváček, J. Skřivánek, Heat and mass transfer in monolithic honeycomb catalysts-I., Chem. Eng. Sci. 30 (1975) 117–123. https://doi.org/10.1016/0009-2509(75)85122-0.

[31] M.T. Kreutzer, P. Du, J.J. Heiszwolf, F. Kapteijn, J.A. Moulijn, Mass transfer characteristics of three-phase monolith reactors, Chem. Eng. Sci. 56 (2001) 6015–6023. https://doi.org/10.1016/S0009-2509(01)00271-8.

[32] S. Roy, A. K. Heibel, W. Liu, T. Boger, Design of monolithic catalysts for multiphase reactions, Chem. Eng. Sci. 59 (2004) 957–966. https://doi.org/10.1016/j.ces.2003.12.001.

[33] L. Giani, G. Groppi, E. Tronconi, Mass-transfer characterization of metallic foams as supports for structured catalysts, Ind. Eng. Chem. Res. 44 (2005) 4993–5002. https://doi.org/10.1021/ie0490886.

[34] M. V. Twigg, J.T. Richardson, Theory and applications of ceramic foam catalysts, Chem. Eng. Res. Des. 80 (2002) 183–189. https://doi.org/10.1016/S0263-8762(02)72166-7.

[35] F. Lucci, A. Della Torre, J. von Rickenbach, G. Montenegro, D. Poulikakos, P. Dimopoulos Eggenschwiler, Performance of randomized Kelvin cell structures as catalytic substrates: Mass-transfer based analysis, Chem. Eng. Sci. 112 (2014) 143–151. https://doi.org/10.1016/j.ces.2014.03.023.

[36] C. Sinn, J. Wentrup, G.R. Pesch, J. Thöming, L. Kiewidt, Structure-heat transport analysis of periodic open-cell foams to be used as catalyst carriers, Chem. Eng. Res. Des. 166 (2021) 209–219. https://doi.org/10.1016/j.cherd.2020.12.007.

[37] S. Wójcik, G. Ercolino, M. Gajewska, C.W. Moncada Quintero, S. Specchia, A. Kotarba, Robust Co_3O_4|α-Al_2O_3|cordierite structured catalyst for N_2O abatement – Validation of the SCS method for active phase synthesis and deposition, Chem. Eng. J. 377 (2018) 120088. https://doi.org/10.1016/j.cej.2018.10.025.

[38] A. Vita, C. Italiano, L. Pino, M. Laganà, M. Ferraro, V. Antonucci, High-temperature CO_2 methanation over structured Ni/GDC catalysts: Performance and scale-up for

Power-to-Gas application, Fuel Process. Technol. 202 (2020) 106365. https://doi.org/10.1016/j.fuproc.2020.106365.

[39] A. Egana, O. Sanz, D. Merino, X. Moriones, M. Montes, Fischer-Tropsch Synthesis Intensification in Foam Structures, Ind. Eng. Chem. Res. 57 (2018) 10187–10197. https://doi.org/10.1021/acs.iecr.8b01492.

[40] A. Cybulski, J.A. Moulijn, Structured Catalysts and Reactors, Marcel Dekker, Inc., New York, 1998.

[41] A.I. Stankiewicz, J.A. Moulijn, Process Intensification: Transforming Chemical Engineering, AIChE - Chem. Eng. Prog. 96 (2000) 22–33. https://www.aiche.org/sites/default/files/docs/news/010022_cep_stankiewicz.pdf.

[42] T.J. Lu, H.A. Stone, M.F. Ashby, Heat transfer in open-cell metal foams, Acta Mater. 46 (1998) 3619–3635. https://doi.org/10.1016/S1359-6454(98)00031-7.

[43] W.Y. Jang, A.M. Kraynik, S. Kyriakides, On the microstructure of open-cell foams and its effect on elastic properties, Int. J. Solids Struct. 45 (2008) 1845–1875. https://doi.org/10.1016/j.ijsolstr.2007.10.008.

[44] F.C. Buciuman, B. Kraushaar-Czarnetzki, Ceramic Foam Monoliths as Catalyst Carriers. 1. Adjustment and Description of the Morphology, Ind. Eng. Chem. Res. 42 (2003) 1863–1869. https://doi.org/10.1021/ie0204134.

[45] E. Tronconi, G. Groppi, C.G. Visconti, Structured catalysts for non-adiabatic applications, Curr. Opin. Chem. Eng. 5 (2014) 55–67. https://doi.org/10.1016/j.coche.2014.04.003.

[46] S. Voltolina, P. Marín, F.V. Díez, S. Ordóñez, Open-cell foams as beds in multiphase reactors: Residence time distribution and mass transfer, Chem. Eng. J. 316 (2017) 323–331. https://doi.org/10.1016/j.cej.2017.01.113.

[47] A.M. Dashliborun, A. Füssel, F. Larachi, Prospect of open-cell solid foams for

floating-platform multiphase reactor applications – Maldistribution susceptibility and hydrodynamic behavior, Chem. Eng. J. 332 (2018) 596–607. https://doi.org/10.1016/j.cej.2017.09.116.

[48] A. Inayat, M. Klumpp, M. Lämmermann, H. Freund, W. Schwieger, Development of a new pressure drop correlation for open-cell foams based completely on theoretical grounds: Taking into account strut shape and geometric tortuosity, Chem. Eng. J. 287 (2016) 704–719. https://doi.org/10.1016/j.cej.2015.11.050.

[49] A. Aguirre, V. Chandra, E.A.J.F. Peters, J.A.M. Kuipers, M.F. Neira D'Angelo, Open-cell foams as catalysts support: A systematic analysis of the mass transfer limitations, Chem. Eng. J. 393 (2020) 124656. https://doi.org/10.1016/j.cej.2020.124656.

[50] C.W. Moncada Quintero, R.Z. Babar, S. Specchia, Performance and Controlling Regimes Analysis of Methane Steam Reforming on Ru/γ-Al_2O_3 Cordierite Monoliths, Green Energy Technol. (2021) 91–131. https://doi.org/10.1007/978-981-15-5667-8_5.

[51] P. Bernard, P. Stelmachowski, P. Broś, W. Makowski, A. Kotarba, Demonstration of the Influence of Specific Surface Area on Reaction Rate in Heterogeneous Catalysis, J. Chem. Educ. 98 (2021) 935–940. https://doi.org/10.1021/acs.jchemed.0c01101.

[52] C.W. Moncada Quintero, G. Ercolino, A. Poozhikunnath, R. Maric, S. Specchia, Analysis of heat and mass transfer limitations for the combustion of methane emissions on PdO/Co_3O_4 coated on ceramic open cell foams, Chem. Eng. J. 405 (2021) 126970. https://doi.org/10.1016/j.cej.2020.126970.

[53] C.W. Moncada Quintero, G. Ercolino, S. Specchia, Effect of the Co_3O_4 load on the performance of PdO/Co_3O_4/ZrO_2 open cell foam catalysts for the lean combustion of methane: kinetic and mass transfer regimes, Catal. Today. (2021). https://doi.org/10.1016/j.cattod.2021.03.014.

[54] G. Ercolino, P. Stelmachowski, S. Specchia, Catalytic Performance of Pd/Co_3O_4 on

SiC and ZrO_2 Open Cell Foams for Process Intensification of Methane Combustion in Lean Conditions, Ind. Eng. Chem. Res. 56 (2017) 6625–6636. https://doi.org/10.1021/acs.iecr.7b01087.

[55] G. Ercolino, S. Karimi, P. Stelmachowski, S. Specchia, Catalytic combustion of residual methane on alumina monoliths and open cell foams coated with Pd/Co_3O_4, Chem. Eng. J. 326 (2017) 339–349. https://doi.org/10.1016/j.cej.2017.05.149.

[56] P.A. Carlsson, M. Skoglundh, E. Fridell, E. Jobson, B. Andersson, Induced low temperature catalytic ignition by transient changes in the gas composition, Catal. Today. 73 (2002) 307–313. https://doi.org/10.1016/j.cej.2010.10.051.

[57] R.H. Nibbelke, J.H.B.J. Hoebink, G.B. Marin, Kinetically induced multiplicity of steady states in integral catalytic reactors, Chem. Eng. Sci. 53 (1998) 2195–2210. https://doi.org/10.1016/S0009-2509(98)00055-4.

[58] S. Specchia, S. Tacchino, V. Specchia, Facing the catalytic combustion of CH_4/H_2 mixtures into monoliths, Chem. Eng. J. 167 (2011) 622–633. https://doi.org/10.1016/j.cej.2010.10.051.

[59] A. Aseem, G.G. Jeba, M.T. Conato, J.D. Rimer, M.P. Harold, Oxidative coupling of methane over mixed metal oxide catalysts: Steady state multiplicity and catalyst durability, Chem. Eng. J. 331 (2018) 132–143. https://doi.org/10.1016/j.cej.2017.08.093.

[60] L.A. Vandewalle, R. Van de Vijver, K.M. Van Geem, G.B. Marin, The role of mass and heat transfer in the design of novel reactors for oxidative coupling of methane, Chem. Eng. Sci. 198 (2019) 268–289. https://doi.org/10.1016/j.ces.2018.09.022.

[61] C.W. Moncada Quintero, M. Servel, F. Augier, Y. Haroun, J.-F. Joly, S. Specchia, Imaging ceramic open cell foams by X-ray micro computed tomography, Ind. Eng. Chem. Res. submitted (2021).

[62] I. Cornejo, P. Nikrityuk, R.E. Hayes, Heat and mass transfer inside of a monolith honeycomb: From channel to full size reactor scale, Catal. Today. (2020). https://doi.org/10.1016/j.cattod.2020.10.036.

[63] J.J. Carberry, Chemical and Catalytic Reaction Engineering, McGraw-Hill, New York, 1976.

[64] J.R. Anderson, M. Boudart, Catalysis Science and Technology, 1987. https://doi.org/10.1007/978-3-642-93278-6_1.

[65] C. Mcgreavy, L. Draper, E.K.T. Kam, Methodologies for the design of reactors using structured catalysts: modelling and experimental study of diffusion and reaction in structured catalysts, Chem. Eng. Sci. 49 (1994). https://doi.org/10.1016/0009-2509(94)00384-X.

[66] S. Roy, T. Bauer, M. Al-Dahhan, P. Lehner, T. Turek, Monoliths as multiphase reactors: A review, AIChE J. 50 (2004) 2918–2938. https://doi.org/10.1002/aic.10268.

[67] O.P. Klenov, S.A. Pokrovskaya, N.A. Chumakova, S.N. Pavlova, V.A. Sadykov, A.S. Noskov, Effect of mass transfer on the reaction rate in a monolithic catalyst with porous walls, Catal. Today. 144 (2009) 258–264. https://doi.org/10.1016/j.cattod.2008.11.014.

[68] A. Gancarczyk, M. Iwaniszyn, M. Piatek, M. Korpyś, K. Sindera, P.J. Jodłowski, J. Łojewska, A. Kołodziej, Catalytic Combustion of Low-Concentration Methane on Structured Catalyst Supports, Ind. Eng. Chem. Res. 57 (2018) 10281–10291. https://doi.org/10.1021/acs.iecr.8b01987.

[69] V. Balakotaiah, On the relationship between Aris and Sherwood numbers and friction and effectiveness factors, Chem. Eng. Sci. 63 (2008) 5802–5812. https://doi.org/10.1016/j.ces.2008.08.025.

[70] S.Y. Joshi, M.P. Harold, V. Balakotaiah, Low-Dimensional Models for Real Time

Simulations of Catalytic Monoliths, AIChE J. 55 (2009) 1771–1783. https://doi.org/10.1002/aic.11794.

[71] S.Y. Joshi, M.P. Harold, V. Balakotaiah, On the use of internal mass transfer coefficients in modeling of diffusion and reaction in catalytic monoliths, Chem. Eng. Sci. 64 (2009) 4976–4991. https://doi.org/10.1016/j.ces.2009.08.008.

[72] S.Y. Joshi, M.P. Harold, V. Balakotaiah, Overall mass transfer coefficients and controlling regimes in catalytic monoliths, Chem. Eng. Sci. 65 (2010) 1729–1747. https://doi.org/10.1016/j.ces.2009.11.021.

[73] S.Y. Joshi, Y. Ren, M.P. Harold, V. Balakotaiah, Determination of kinetics and controlling regimes for H2 oxidation on Pt/Al_2O_3 monolithic catalyst using high space velocity experiments, Appl. Catal. B Environ. 102 (2011) 484–495. https://doi.org/10.1016/j.apcatb.2010.12.030.

[74] G. Incera Garrido, F.C. Patcas, S. Lang, B. Kraushaar-Czarnetzki, Mass transfer and pressure drop in ceramic foams: A description for different pore sizes and porosities, Chem. Eng. Sci. 63 (2008) 5202–5217. https://doi.org/10.1016/j.ces.2008.06.015.

[75] M. Bhattacharya, M.P. Harold, V. Balakotaiah, Mass-transfer coefficients in washcoated monoliths, AIChE J. 50 (2004) 2939–2955. https://doi.org/10.1002/aic.10212.

[76] L.B. Younis, R. Viskanta, Experimental determination of the volumetric heat transfer coefficient between stream of air and ceramic foam, Int. J. Heat Mass Transf. 36 (1993) 1425–1434. https://doi.org/10.1016/S0017-9310(05)80053-5.

[77] D.E. Mears, Diagnostic criteria for heat transport limitations in fixed bed reactors, J. Catal. 20 (1971) 127–131. https://doi.org/10.1016/0021-9517(71)90073-X.

[78] J.B. Anderson, A criterion for isothermal behaviour of a catalyst pellet, Chem. Eng. Sci. 18 (1963) 147–148.

[79] J.M. Smith, Chemical Engineering Kinetics, 2nd ed., McGraw-Hill, New York, 1970.

[80] G.F. Froment, K.B. Bischoff, J. De Wilde, Chemical Reactor Analysis and Design, 3rd ed., John Wiley & Sons, New York, 2011.

[81] B.R. Bird, W.E. Stewart, E.N. Lightfoot, Transport Phenomena, 2nd ed., Wiley, 2006.

[82] G. Groppi, C. Cristiani, L. Lietti, P. Forzatti, Study of PdO/Pd transformation over alumina supported catalysts for natural gas combustion, Stud. Surf. Sci. Catal. 130 (2000) 3801–3806. https://doi.org/10.1016/s0167-2991(00)80615-1.

[83] L.M.T. Simplício, S.T. Brandão, D. Domingos, F. Bozon-Verduraz, E.A. Sales, Catalytic combustion of methane at high temperatures: Cerium effect on PdO/Al_2O_3 catalysts, Appl. Catal. A Gen. 360 (2009) 2–7. https://doi.org/10.1016/j.apcata.2009.03.005.

[84] S. Colussi, P. Fornasiero, A. Trovarelli, Structure-activity relationship in Pd/CeO_2 methane oxidation catalysts, Chinese J. Catal. 41 (2020) 938–950. https://doi.org/10.1016/S1872-2067(19)63510-2.

[85] J. Lin, X. Chen, Y. Zheng, F. Huang, Y. Xiao, Y. Zheng, L. Jiang, Facile construction of ultrastable alumina anchored palladium catalysts: via a designed one pot strategy for enhanced methane oxidation, Catal. Sci. Technol. 10 (2020) 4612–4623. https://doi.org/10.1039/d0cy00727g.

[86] S. Nasr, N. Semagina, R.E. Hayes, Kinetic Modelling of Co_3O_4- and Pd/Co_3O_4-Catalyzed Wet Lean Methane Combustion, Emiss. Control Sci. Technol. 6 (2020) 269–278. https://doi.org/10.1007/s40825-019-00143-0.

[87] G.S. Bugosh, V.G. Easterling, I.A. Rusakova, M.P. Harold, Anomalous steady-state and spatio-temporal features of methane oxidation on $Pt/Pd/Al_2O_3$ monolith spanning lean and rich conditions, Appl. Catal. B Environ. 165 (2015) 68–78. https://doi.org/10.1016/j.apcatb.2014.09.058.

[88] A.K. Datye, J. Bravo, T.R. Nelson, P. Atanasova, M. Lyubovsky, L. Pfefferle, Catalyst microstructure and methane oxidation reactivity during the Pd↔PdO transformation on alumina supports, Appl. Catal. A Gen. 198 (2000) 179–196. https://doi.org/10.1016/S0926-860X(99)00512-8.

[89] D. Ciuparu, M.R. Lyubovsky, E. Altman, L.D. Pfefferle, A. Datye, Catalytic combustion of methane over palladium-based catalysts, Catal. Rev. - Sci. Eng. 44 (2002) 593–649. https://doi.org/10.1081/CR-120015482.

[90] S. Colussi, A. Trovarelli, E. Vesselli, A. Baraldi, G. Comelli, G. Groppi, J. Llorca, Structure and morphology of Pd/Al_2O_3 and $Pd/CeO_2/Al_2O_3$ combustion catalysts in Pd-PdO transformation hysteresis, Appl. Catal. A Gen. 390 (2010) 1–10. https://doi.org/10.1016/j.apcata.2010.09.033.

[91] R. Gholami, M. Alyani, K.J. Smith, Deactivation of Pd catalysts by water during low temperature methane oxidation relevant to natural gas vehicle converters, 2015. https://doi.org/10.3390/catal5020561.

[92] Y.H.C. Chin, M. García-Diéguez, E. Iglesia, Dynamics and thermodynamics of Pd-PdO phase transitions: Effects of pd cluster size and kinetic implications for catalytic methane combustion, J. Phys. Chem. C. 120 (2016) 1446–1460. https://doi.org/10.1021/acs.jpcc.5b06677.

[93] R.J. Farrauto, M.C. Hobson, T. Kennelly, E.M. Waterman, Catalytic chemistry of supported palladium for combustion of methane, Appl. Catal. A, Gen. 81 (1992) 227–237. https://doi.org/10.1016/0926-860X(92)80095-T.

[94] H. Scott Fogler, Elements of chemical reaction engineering, 5^{th} ed., Pearson Education, Inc., Kendallville, Indiana (USA), 2016.

[95] B. Dietrich, Heat transfer coefficients for solid ceramic sponges-Experimental results and correlation, Int. J. Heat Mass Transf. 61 (2013) 627–637.

https://doi.org/10.1016/j.ijheatmasstransfer.2013.02.019.

[96] X.L. Xia, X. Chen, C. Sun, Z.H. Li, B. Liu, Experiment on the convective heat transfer from airflow to skeleton in open-cell porous foams, Int. J. Heat Mass Transf. 106 (2017) 83–90. https://doi.org/10.1016/j.ijheatmasstransfer.2016.10.053.

[97] V. Specchia, G. Baldi, S. Sicardi, Heat transfer in packed bed reactors with one phase flow, Chem. Eng. Commun. 4 (1980) 361–380. https://doi.org/10.1080/00986448008935916.

[98] C.G. Visconti, E. Tronconi, G. Groppi, L. Lietti, M. Iovane, S. Rossini, R. Zennaro, Monolithic catalysts with high thermal conductivity for the Fischer-Tropsch synthesis in tubular reactors, Chem. Eng. J. 171 (2011) 1294–1307. https://doi.org/10.1016/j.cej.2011.05.014.

[99] O. Sanz, I. Velasco, I. Reyero, I. Legorburu, G. Arzamendi, L.M. Gandía, M. Montes, Effect of the thermal conductivity of metallic monoliths on methanolsteam reforming, Catal. Today. 273 (2016) 131–139. https://doi.org/10.1016/j.cattod.2016.03.008.